

An Effective Model of the Retinoic Acid Induced HL-60 Differentiation Program

Ryan Tasseff, Holly A. Jensen, Johanna Congleton[†], Wei Dai, Katherine Rogers, Adithya Sagar, Rodica P. Bunaciu[†], Andrew Yen[†], and Jeffrey D. Varner*

Robert Frederick Smith School of Chemical and Biomolecular Engineering and [†]Department of Biomedical Sciences, Cornell University, Ithaca NY 14853

Running Title: Effective modeling of HL-60 differentiation

To be submitted: ?

*Corresponding author:

Jeffrey D. Varner,

Professor, Robert Frederick Smith School of Chemical and Biomolecular Engineering,
244 Olin Hall, Cornell University, Ithaca NY, 14853

Email: jdv27@cornell.edu

Phone: (607) 255 - 4258

Fax: (607) 255 - 9166

Abstract

In this study, we present an effective model All-Trans Retinoic Acid (ATRA)-induced differentiation of HL-60 cells. The model describes a key architectural feature of ATRA-induced differentiation, positive feedback between an ATRA-inducible signalsome complex involving many proteins including Vav1, a guanine nucleotide exchange factor, and the activation of the mitogen activated protein kinase (MAPK) cascade. The model, which was developed by integrating logical rules with kinetic modeling, was significantly smaller than previous models. However, despite its simplicity, it captured key features of ATRA induced differentiation of HL-60 cells. We identified an ensemble of effective model parameters using measurements taken from ATRA-induced HL-60 cells. Using these parameters, model analysis predicted that MAPK activation was bistable as a function of ATRA exposure. Conformational experiments supported ATRA-induced bistability. These findings, combined with other literature evidence, suggest that positive feedback is central to a diversity of cell fate programs.

1 Introduction

2 Understanding the architecture of differentiation programs is an important therapeutic
3 challenge. Differentiation induction chemotherapy (DIC), using agents such as the vita-
4 min A derivative all-trans retinoic acid (ATRA), is a promising approach for the treatment
5 of many cancers (1–3). For example, ATRA treatment induces remission in 80–90% of
6 promyelocytic leukemia (APL) PML-RAR α -positive patients (4), thereby transforming a
7 fatal diagnosis into a manageable disease. However, remission is sometimes not durable
8 and relapsed cases exhibit emergent ATRA resistance (5, 6). To understand the basis of
9 this resistance, we must first understand the ATRA-induced differentiation program. To-
10 ward this challenge, lessons learned in model systems, such as the lineage-uncommitted
11 human myeloblastic cell line HL-60, could inform our analysis of the more complex dif-
12 ferentiation programs occurring in patients. Patient derived HL-60 leukemia cells have
13 been a durable experimental model since the 1970's to study differentiation (7). HL-60
14 undergoes cell cycle arrest and either myeloid or monocytic differentiation following stim-
15 ulation; ATRA induces G1/G0-arrest and myeloid differentiation in HL-60 cells, while 1,25-
16 dihydroxy vitamin D3 (D3) induces arrest and monocytic differentiation. Commitment to
17 cell cycle arrest and differentiation requires approximately 48 hr of treatment, during which
18 HL-60 cells undergo two division cycles.

19 Sustained mitogen-activated protein kinase (MAPK) activation is a defining feature of
20 ATRA-induced HL-60 differentiation. ATRA drives sustained MEK-dependent activation
21 of the Raf/MEK/ERK pathway, leading to arrest and differentiation (8). MEK inhibition re-
22 sults in the loss of ERK and Raf phosphorylation, and the failure to arrest and differentiate
23 (9). ATRA (and its metabolites) are ligands for the hormone activated nuclear transcrip-
24 tion factors retinoic acid receptor (RAR) and retinoid X receptor (RXR) (10). RAR/RXR
25 activation is necessary for ATRA-induced Raf phosphorylation (9), and the formation of
26 an ATRA-inducible signalsome complex at the membrane which drives MAPK activation

27 through a yet to be identified kinase activity. While the makeup of the signalsome com-
28 plex is not yet known, we do know that it is composed of Src family kinases Fgr and Lyn,
29 PI3K, c-Cbl, Slp76, and KSR, as well as IRF-1 transcription factors (11–15). Signalsome
30 formation and activity is driven by ATRA-induced expression of CD38 and the putative
31 heterotrimeric Gq protein-coupled receptor BLR1 (16, 17). BLR1, identified as an early
32 ATRA (or D3)-inducible gene using differential display (18), is necessary for MAPK ac-
33 tivation and differentiation (17), and is also involved with signalsome activity. Studies
34 of the BLR1 promoter identified a 5' 17bp GT box approximately 1 kb upstream of the
35 transcriptional start that conferred ATRA responsiveness (17). Members of the BLR1
36 transcriptional activator complex, e.g. NFATc3 and CREB, are phosphorylated by ERK,
37 JNK or p38 MAPK family members suggesting positive feedback between the signalsome
38 and MAPK activation (19). BLR1 overexpression enhanced Raf phosphorylation and ac-
39 celerated terminal differentiation, while Raf inhibition reduced BLR1 expression and dif-
40 ferentiation (20). BLR1 knock-out cells failed to activate Raf or differentiate in the pres-
41 ence of ATRA (20). Interestingly, both the knockdown or inhibition of Raf, also reduced
42 BLR1 expression and functional differentiation (20). Thus, the expression of signalsome
43 components e.g., BLR1 was Raf dependent, while Raf activation depended upon the sig-
44 nalsome. A recent computational study of ATRA-induced differentiation in HL-60 cells
45 suggested that the BLR1-MAPK positive feedback circuit was sufficient to explain ATRA-
46 induced sustained MAPK activation, and the expression of a limited number of functional
47 differentiation markers (21). Model analysis also suggested that Raf was the most distinct
48 of the MAPK proteins. However, this previous study developed and analyzed a complex
49 model, thus leaving open the critical question of what is the minimal positive feedback
50 circuit required to drive ATRA-induced differentiation.

51 In this study, we explored this question using a minimal mathematical model of the
52 key architectural feature of ATRA induced differentiation of HL-60 cells, namely positive

53 feedback between an ATRA-inducible signalsome complex and MAPK activation. The
54 ATRA responsive signalsome-MAPK circuit was then used to drive a downstream gene
55 expression program which encoded for the expression of functional differentiation mark-
56 ers. The effective model used a novel framework which integrated logical rules with ki-
57 netic modeling to describe gene expression and protein regulation, while largely relying
58 upon biophysical parameters from the literature. This formulation significantly reduced
59 the size and complexity of the model compared to the previous study of Tasseff et al.,
60 while increasing the breadth of the biology described (21). The effective model, despite
61 its simplicity, captured key features of ATRA induced differentiation of HL-60 cells. Model
62 analysis predicted the bistability of MAPK activation as a function of ATRA exposure; con-
63 formational experiments supported ATRA-induced bistability. Model simulations were also
64 consistent with measurements of the influence of MAPK inhibitors, and the failure of BLR1
65 knockout cells to differentiate when exposed to ATRA. Lastly, we showed by through im-
66 munoprecipitation studies, that the guanine nucleotide exchange factor Vav1 is potentially
67 a new ATRA-inducible member of the signalsome complex. Taken together, these findings
68 when combined with other literature evidence, suggested that positive feedback architec-
69 tures are central to differentiation programs generally, and necessary for ATRA-induced
70 differentiation.

71 **Results**

72 We constructed an effective model of ATRA-induced HL-60 differentiation which described
73 signaling and gene expression events following the addition of ATRA (Fig. 1). The model
74 connectivity was developed from literature and the studies presented here (Table 1). We
75 decomposed the ATRA program into three modules; a signal initiation module that sensed
76 and transformed the ATRA signal into activated cRaf-pS621 and the ATRA-RXR/RAR
77 (Trigger) signals (Fig. 1A); a signal integration module that controlled the expression of
78 upstream transcription factors given cRaf-pS621 and activated Trigger signals (Fig. 1B);
79 and a phenotype module which encoded the expression of functional differentiation mark-
80 ers from the ATRA-inducible transcription factors (Fig. 1C). Each component of these
81 modules was described by a mRNA and protein balance equation. Additionally, the sig-
82 nal initiation module also described the abundance of activated species e.g., Trigger and
83 cRaf-pS621 whose values were derived from unactivated Trigger and cRaf protein levels.
84 Lastly, because the population of HL-60 cells was dividing (at least before ATRA-induced
85 cell cycle arrest), we also considered a dilution term in all balance equations. The sig-
86 nal initiation module contained nine differential equations, while the signal integration and
87 phenotype modules were collectively encoded by 54 differential equations. Model param-
88 eters were taken literature (Table 2), or estimated from experimental data using heuristic
89 optimization (see materials and methods).

90 The signal initiation module recapitulated sustained signalsome and MAPK activation
91 following exposure to $1\mu\text{M}$ ATRA (Fig. 2A-B). An ensemble of effective model param-
92 eters was estimated by minimizing the difference between simulations and time-series
93 measurements of BLR1 mRNA and cRaf-pS621 following the addition of $1\mu\text{M}$ ATRA. We
94 focused on the S621 phosphorylation site of cRaf since enhanced phosphorylation at
95 this site is a defining characteristic of sustained MAPK activation in HL-60. The effective
96 model captured both ATRA-induced BLR1 expression (Fig. 2A) and sustained phospho-

97 phosphorylation of cRaf-pS621 (Fig. 2B) in a growing population of HL-60 cells. Together, the
98 reinforcing positive feedback between the signalsome and MAPK led to sustained activation
99 over multiple cellular generations. However, the effective model failed to capture the
100 decline of BLR1 message after 48 hr of ATRA exposure. This suggested that we captured
101 the logic leading to the onset of differentiation, but failed to describe program shutdown.
102 Next, we tested the response of the signal initiation module to different ATRA dosages.

103 The signal initiation model was bistable with respect to ATRA induction (Fig. 2C-D).
104 Phaseplane analysis predicted two stable steady-states when ATRA was present below
105 a critical threshold, and only a single steady-state above the threshold (Fig. 2C). In the
106 lower stable state, neither the signalsome nor cRaf-pS621 were present (thus, the differ-
107 entiation program was deactivated). However, at the high stable state, both the signal-
108 some and cRaf-pS621 were present, allowing for sustained activation and differentiation.
109 Interestingly, when ATRA was above a critical threshold, only the activated state was ac-
110 cessible (Fig. 2D). To test these findings, we first identified the ATRA threshold. We
111 exposed HL-60 cells to different ATRA concentrations for 72 hr (Fig. 2E). Morphological
112 changes associated with differentiation were visible for ATRA \geq 0.25 μ M, suggesting the
113 critical ATRA threshold was near this concentration. Next, we conducted ATRA washout
114 experiments to determine if activated cells remained activated in the absence of ATRA.
115 HL-60 cells locked into an activated state remained activated following ATRA withdraw-
116 (Fig. 3). This sustained activation resulted from reinforcing feedback between the sig-
117 nalsome and the MAPK pathway. Thus, following activation, if we inhibited or removed
118 elements from the signal initiation module we expected the signalsome and MAPK signals
119 to decay. We simulated ATRA induced activation in the presence of kinase inhibitors, and
120 without key circuit elements. Consistent with experimental results using multiple MAPK
121 inhibitors, ATRA activation in the presence of MAPK inhibitors lowered the steady-state
122 value of signalsome (Fig. 3A). In the presence of BLR1, the signalsome and cRaf-pS621

signals were maintained following ATRA withdraw (Fig. 3B, gray). On the other hand, BLR1 deletion removed the ability of the circuit to maintain a sustained MAPK response following the withdraw of ATRA (Fig. 3B, blue). Lastly, washout experiments in which cells were exposed to $1\mu\text{M}$ ATRA for 24 hr, and then transferred to fresh media without ATRA, confirmed the persistence of the self sustaining activated state for up to 144 hr (Fig. 3C). Thus, these experiments confirmed that reinforcing positive feedback likely drives the ATRA-induced differentiation program. Next, we analyzed the ATRA-induced downstream gene expression program following signalsome and cRaf activation.

The signal integration and phenotype modules described ATRA-induced gene expression in wild-type HL-60 cells (Fig. 4). The signal initiation module produced two outputs, activated Trigger and cRaf-pS621 which drove the expression of ATRA-induced transcription factors, which then in turn activated the phenotypic program. In particular, Trigger (a surrogate for the RAR α /RXR transcriptional complex) regulated the expression of the transcription factors CCATT/enhancer binding protein α (C/EBP α), PU.1, and Egr-1. In turn, these transcription factors, in combination with cRaf-pS621, regulated the expression of downstream phenotypic markers such as CD38, CD11b or p47Phox. We assembled the connectivity of the signal integration and phenotypic programs driven by Trigger and cRaf-pS621 from literature (Table 1). We estimated the parameters for the signal initiation, and phenotype modules from steady-state and dynamic measurements of transcription factor and phenotypic marker expression following the addition of ATRA (22–25). However, the bulk of the model parameters were taken from directly from literature (26) and were not estimated in this study (see materials and methods). The model simulations captured the time dependent expression of CD38 and CD11b following the addition ATRA (Fig. 4A), and the steady-state for signal integration and phenotypic markers (Fig. 4B). Lastly, we used the *predicted* values of the p21 and E2F protein abundance to estimate a black-box model of ATRA-induced G0 arrest (Fig. 5). The phenotype module predicted p21

149 expression significantly increased and E2F expression decreased, in response to ATRA
150 exposure (Fig. 5A). We then used the ratio of these values in a polynomial model to cal-
151 culate the fraction of HL-60 cells in G0 arrest following the addition of ATRA (Fig. 5B). The
152 third-order polynomial model captured the trend in measured G0-arrest values as a func-
153 tion of time, and was robust to uncertainty in the measured data (Fig. 5B, gray). Taken
154 together, the output of the signal integration and phenotypic modules was consistent with
155 time-series and steady-state measurements, thereby validating the assumed molecular
156 connectivity. Moreover, outputs from the phenotype module described the trend in ATRA-
157 induced G0 cell cycle arrest. Next, we explored which nodes and interactions between
158 nodes in the signal integration module most influenced the system response.

159 The Gfi-1 and PPARg proteins were important regulators of ATRA-induced signal in-
160 tegration and phenotypic change (Fig. 6). We conducted pairwise gene knockout simula-
161 tions in the signal integration and phenotype modules to estimate which nodes controlled
162 the processing of the Trigger and cRaF-S621 signals. The difference between the sys-
163 tem state with and without the gene knockouts (encoded as a normalized state displace-
164 ment matrix) was decomposed using Singular Value Decomposition (SVD). A panel of
165 ten parameter sets was sampled, and the average normalized displacement matrix was
166 decomposed. The first six modes (approximately 36% of the total) described >95% of the
167 gene knockout variance, with the most important components of these modes being the
168 Gfi-1 and PPARg proteins, and to a lesser extent PU.1, C/EBPa and AP1 (Fig. 6A).
169 To better understand which protein-DNA connections were important, we simulated the
170 pairwise deletion of interactions between these proteins and their respective regulatory
171 targets. SVD decomposition of the normalized state displacement matrix assembled from
172 the pairwise connection deletions, suggested the first six modes (approximately 26% of
173 the total) accounted for >90% of the variance. Globally, the most sensitive interactions
174 controlled p21 and p47Phox expression, markers for cell-cycle arrest and reactive oxygen

175 formation phenotypic axes activated following ATRA addition (Fig. 6B). Analysis of the
176 modes suggested the action of PPARg, Gfi-1 and C/EBPa were consistently important
177 over multiple target genes. The connection knockout analysis also revealed robustness
178 in the network. For example, no pair of deletions qualitatively changed the expression of
179 regulators such as PU.1, Oct1, Oct4 or PPARg. Thus, the expression of these species
180 was robust to disturbance in the connectivity. To better understand the combined influ-
181 ence of the PPARg and Gfi-1 deletions, we computed the fold change in the protein levels
182 in the single (Δ Gfi-1 or Δ PPARg) and double (Δ Gfi-1 and Δ PPARg) mutants for the best
183 fit parameter set (Fig. 7). Deletion of Gfi-1 led to a 2-4 fold increase in EGR-1, CD11b
184 and C/EBPa expression, and a >8 fold increase in PU.1 abundance (Fig. 7,blue). On
185 the other hand, deletion of PPARg led to >8 fold downregulation of CD38, p21, IRF1
186 and OCT1 (Fig. 7,red). Both knockouts slightly increased E2F expression, but neither
187 influenced the expression of p47Phox. The double mutant was qualitatively similar to the
188 combined behavior of the two single mutant cases. Taken together, Gfi-1 and PPARg
189 controlled the cell-cycle arrest and receptor signaling axes, with PPARg regulating CD38,
190 IRF1 and p21 expression while Gfi-1 controlled CD11b expression. These simulations
191 suggested deletion of PPARg and Gfi-1 would not interfere with reactive oxygen forma-
192 tion, but would limit the ability of HL-60 cells to arrest. However, this analysis did not
193 give insight into which components upstream of the signal initiation module were impor-
194 tant. Toward this question, we explored the composition and regulation of the signalsome
195 complex by experimentally interrogating a panel of possible Raf interaction partners.

196 The composition of the signalsome, and the kinase ultimately responsible for medi-
197 ating ATRA-induced Raf activation is currently unknown. To explore this question, we
198 conducted immunoprecipitation and subsequent Western blotting to identify physical in-
199 teractions between Raf and 19 putative interaction partners. A panel of 19 possible Raf
200 interaction partners (kinases, GTPases, scaffolding proteins etc) was constructed based

upon known signaling pathways. We did not consider the most likely binding partner, the small GTPase RAS, as previous studies have ruled it out in MAPK activation in HL-60 cells (20, 27). Total Raf was used as a bait protein for the immunoprecipitation studies. Interrogation of the Raf interactome suggested Vav1 was involved with ATRA-induced initiation of MAPK activity (Fig. 8). Western blot analysis using total Raf and pS621 Raf specific antibodies confirmed the presence of the bait protein, total and phosphorylated forms, in the immunoprecipitate (Fig. 8A). Of the 19 proteins sampled, Vav1, Src, CK2, Akt, and 14-3-3 precipitated with Raf, suggesting a direct physical interaction was possible. However, only the associations between Raf and Vav1 and Raf and Src were ATRA-inducible (Fig. 8). Furthermore, the Vav1 and Src associations were correlated with pS621 Raf abundance in the precipitate. Others proteins e.g., CK2, Akt and 14-3-3, generally bound Raf regardless of phosphorylation status or ATRA treatment. The remaining 14 proteins were expressed in whole cell lysate (Fig. 8B), but were not detectable in the precipitate of Raf IP. Treatment with the Raf kinase inhibitor GW5074 following ATRA exposure reduced the association of both Vav1 with Raf and Src with Raf (Fig. 8), although the signal intensity for Src was notably weak. However, GW5074 did not influence the association of CK2 or 14-3-3 with Raf, further demonstrating their independence from Raf phosphorylation. Interestingly, the Raf-Akt interaction qualitatively increased following treatment with GW5074; however, it remained unaffected by treatment with ATRA. Src family kinases are known to be important in myeloid differentiation (28) and their role in HL-60 differentiation has been investigated elsewhere (11). Given the existing work and variable reproducibility in the context of the Raf immunoprecipitate, we did not investigate the role of Src further in this study. Taken together, the immunoprecipitation and GW5074 results implicated Vav1 association to be correlated with Raf activation following ATRA-treatment. Previous studies demonstrated that a Vav1-Slp76-Cbl-CD38 complex plays an important role in ATRA-induced MAPK activation and differentiation of HL-60 cells (13). Here we

227 did not observe direct interaction of Raf with Cbl or Slp76; however, this complex could
228 be involved upstream. Next, we considered the effect of the Raf kinase inhibitor GW5074
229 on functional markers of ATRA-induced growth arrest and differentiation.

230 Inhibition of Raf kinase activity modulated MAPK activation and differentiation mark-
231 ers following ATRA exposure (Fig. 8D-F). ATRA treatment alone statistically significantly
232 increased the G1/G0 percentage over the untreated control, while GW5074 alone had a
233 negligible effect on the cell cycle distribution (Fig. 8D). Surprisingly, the combination of
234 GW5074 and ATRA statistically significantly increased the G1/G0 population ($82 \pm 1\%$)
235 compared with ATRA alone ($61 \pm 0.5\%$). Increased G1/G0 arrest following the combined
236 treatment with GW5074 and ATRA was unexpected, as the combination of ATRA and the
237 MEK inhibitor (PD98059) has been shown previously to decrease ATRA-induced growth
238 arrest (8). However, growth arrest is not the sole indication of functional differentiation.
239 Expression of the cell surface marker CD11b has also been shown to coincide with HL-60
240 cells myeloid differentiation (29). We measured CD11b expression, for the various treat-
241 ment groups, using immuno-fluorescence flow cytometry 48 hr post-treatment. As with
242 G1/G0 arrest, ATRA alone increased CD11b expression over the untreated control, while
243 GW5074 further enhanced ATRA-induced CD11b expression (Fig. 8E). GW5074 alone
244 had no statistically significant effect on CD11b expression, compared with the untreated
245 control. Lastly, the inducible reactive oxygen species (ROS) response was used as a func-
246 tional marker of differentiated neutrophils (16). We measured the ROS response induced
247 by the phorbol ester 12-O-tetradecanoylphorbol-13-acetate (TPA) using flow cytometry.
248 Untreated cells showed no discernible TPA response, with only $7.0 \pm 3.0\%$ ROS induction
249 (Fig. 8F). Cells treated with ATRA had a significantly increased TPA response, $53 \pm 7\%$
250 ROS induction 48 hr post-treatment. Treatment with both ATRA and GW5074 statistically
251 significantly reduced ROS induction ($22 \pm 0.6\%$) compared to ATRA alone. Interestingly,
252 Western blot analysis did not detect a GW5074 effect on ATRA-induced expression of

253 p47Phox, a required upstream component of the ROS response (Fig. 8F, bottom). Thus,
254 the inhibitory effect of GW5074 on inducible ROS might occur downstream of p47Phox
255 expression. However, the ROS producing complex is MAPK dependent, therefore it is
256 also possible that GW5074 inhibited ROS production by interfering with MAPK activation
257 (in which case the p47Phox marker might not accurately reflect phenotypic conversion
258 and differentiation).

259 **Discussion**

260 In this study, we presented an effective model of ATRA-inducible differentiation of HL-60
261 cells. The model consisted of three modules: a signal initiation module that sensed and
262 transformed the ATRA signal into activated cRaf-pS621 and the ATRA-RXR/RAR (Trig-
263 ger) signals; a signal integration module that controlled the expression of upstream tran-
264 scription factors given cRaf-pS621 and activated Trigger signals; and a phenotype mod-
265 ule which encoded the expression of functional differentiation markers from the ATRA-
266 inducible transcription factors. The model described the transcription and translation of
267 genes in each module, and signaling events in each module in a growing population of
268 HL-60 cells. Model parameters were largely taken from literature, however, unknown
269 coefficients were estimated from protein measurements in HL-60 cells following ATRA
270 exposure. Despite its simplicity, the effective model captured key features of the ATRA
271 induced differentiation such as sustained MAPK activation, and bistability with respect
272 to ATRA exposure. The model also described the expression of upstream transcription
273 factors which regulated the expression of differentiation markers. Lastly, analysis of the
274 response of the model to perturbations identified PU.1 and AP1 as master regulators of
275 ATRA-induced differentiation. We also reported a new ATRA-inducible component of the
276 signalsome, Vav1. Vav1 is a guanine nucleotide exchange factor for Rho family GTPases
277 that activate pathways leading to actin cytoskeletal rearrangements and transcriptional al-
278 terations (30). The Vav1/Raf association correlated with Raf activity, was ATRA-inducible
279 and decreased after treatment with the Raf inhibitor GW5074.

280 Naturally occurring cell fate decisions often incorporate reinforcing feedback and bista-
281 bility (31, 32). One of the most well studied cell fate circuits is the Mos mitogen-activated
282 protein kinase cascade in *Xenopus* oocytes. This cascade is activated when oocytes are
283 induced by the steroid hormone progesterone (33). The MEK-dependent activation of
284 p42 MAPK stimulates the accumulation of the Mos oncprotein, which in turn activates

285 MEK, thereby closing the feedback loop. This is similar to the signal initiation module
286 presented here; ATRA drives signalsome formation, which activates MAPK, which in turn
287 leads to more signalsome activation. Thus, while HL-60 and *Xenopus* oocytes are vastly
288 different biological models, their cell fate programs share a similar architectural feature.
289 Reinforcing feedback and bistability has also been implicated in hematopoietic cell fate
290 determination. Laslo et al showed that the counter antagonistic repressors, Gfi-1 and
291 Egr-1/2 (whose expression is tuned by PU.1 and C/EBPa), encodes a bistable switch that
292 results in a macrophage, neutrophil or a mixed lineage population depending upon PU.1
293 and C/EBPa expression (32). The current model contained the Gfi-1 and Egr-1/2 agonis-
294 tic switch; however, its significance was unclear for HL-60 cells. The expression of Gfi-1,
295 Egr-1/2, C/EBPa and PU.1 was not consistent with the canonical lineage pattern expected
296 from literature. For example, Egr-1/2 expression (associated with a macrophage lineage)
297 increased, while Gfi-1 expression (associated with a neutrophil lineage) remained con-
298 stant following ATRA exposure. Literature evidence in nonmalignant myelomonocytic fate
299 selection has shown that Gfi-1 and Egr-1/2 promote granulocytic and monocytic differ-
300 entiation, respectively (32). Thus, HL-60 cells, which are a less mature cancer cell line,
301 exhibited a non-canonical expression pattern. Other unrelated cell fate decisions such
302 as programmed cell death have also been suggested to be bistable (34). Still more bio-
303 chemical networks important to human health, for example the human coagulation or
304 complement cascades, also feature strong positive feedback elements (35). Thus, while
305 reinforcing feedback is often undesirable in human engineered systems, it is at the core
306 of a diverse variety of cell fate programs and other networks important to human health.

307 Analysis of the signal integration and phenotype modules suggested that Gfi-1 and
308 PPAR γ regulated distinct phenotypic axes following ATRA exposure. The most signifi-
309 cantly unregulated protein in the Δ Gfi-1 mutant was the PU.1 protein. PU.1, a member
310 of the ets transcription factor family, is a well known regulatory protein in granulocyte

311 and monocyte development (36). The relative level of PU.1 and C/EBPa is thought to
312 regulate macrophage versus neutrophil cell fate decisions in granulocytic macrophage
313 progenitor cells (37). However, in previous studies we showed that PU.1 has additional
314 non-canonical function as it is highly expressed following the addition of ATRA to HL-60
315 cells. Analysis of the model in this study suggested that the C/EBPa dependent interac-
316 tion of PU.1 with the *NCF1* gene, which encodes for the p47Phox protein, was the most
317 sensitive PU.1 connection. p47Phox, also known as neutrophil cytosol factor 1, is one of
318 four cytosolic subunits of the multi-protein NADPH oxidase complex found in neutrophils
319 (38). This enzyme is responsible for reactive oxygen species (ROS) production, a key
320 component of the anti-microbial function of neutrophils. PU.1 also acted in concert with
321 the activator protein 1 (AP-1) transcription factor to regulate p21 expression, a second
322 phenotypic outcome of ATRA-induced differentiation. The AP-1 transcription factor reg-
323 ulates gene expression in response to a variety of stimuli. However, in the context of
324 ATRA-induced differentiation, AP1 has been shown to be inhibited in

325 Immunoprecipitation studies identified a limited number of ATRA-dependent and -
326 independent Raf interaction partners. While we were unable to detect the association
327 of Raf with common kinases and GTPases such as PKC, PKA, p38, Rac and Rho, we
328 did establish potential interactions between Raf and key partners such as Vav1, Src, Akt,
329 CK2 and 14-3-3. All of these partners are known to be associated with Raf activation
330 or function. Src is known to bind Raf through an SH2 domain, and this association has
331 been shown to be dependent of the serine phosphorylation of Raf (39). Thus, an ATRA in-
332 ductible Src/Raf association may be a result of ATRA-induced Raf phosphorylation at S259
333 or S621. We also identified an interaction between Raf and the Ser/Thr kinases Akt and
334 CK2. Akt can phosphorylate Raf at S259, as demonstrated by studies in a human breast
335 cancer line (40). CK2 can also phosphorylate Raf, although the literature has traditionally
336 focused on S338 and not S621 or S259(41). However, neither of these kinase interactions

337 were ATRA-inducible, suggesting their association with Raf alone was not associated with
338 ATRA-induced Raf phosphorylation. The adapter protein 14-3-3 was also constitutively
339 associated with Raf. The interaction between Raf and 14-3-3 has been associated with
340 both S621 and S259 phosphorylation and activity (42). Additionally, the association of
341 Raf with 14-3-3 not only stabilized S621 phosphorylation, but also reversed the S621
342 phosphorylation from inhibitory to activating (43). Finally, we found that Vav1/Raf associ-
343 ation correlated with Raf activity, was ATRA-inducible and decreased after treatment with
344 GW5074. The presence of Vav1 in Raf/Grb2 complexes has been shown to correlate with
345 increased Raf activity in mast cells (44). Furthermore, studies on Vav1 knockout mice
346 demonstrated that the loss of Vav1 resulted in deficiencies of ERK signaling for both T-
347 cells as well as neutrophils (45, 46). Interestingly, while an integrin ligand-induced ROS
348 response was blocked in Vav1 knockout neutrophils, TPA was able to bypass the Vav1
349 requirement and stimulate both ERK phosphorylation and ROS induction (46). In this
350 study, the TPA-induced ROS response was dependent upon Raf kinase activity, and was
351 mitigated by the addition of GW5074. It is possible that Vav1 is downstream of various
352 integrin receptors but upstream of Raf in terms of inducible ROS responses. Vav1 has
353 also been shown to associate with a Cbl-Slp76-CD38 complex in an ATRA-dependent
354 manner; furthermore, transfection of HL-60 cells with Cbl mutants that fail to bind CD38,
355 yet still bind Slp76 and Vav1, prevents ATRA-induced MAPK activation (13). The literature
356 suggest a variety of possible receptor-signaling pathways, which involve Vav1, for MAPK
357 activation; moreover, given the ATRA-inducible association Vav1 may play a direct role in
358 Raf activation.

359 We hypothesized that Vav1 is a member of an ATRA-inducible complex which propels
360 sustained MAPK activation, arrest and differentiation. Initially, ATRA-induced Vav1 ex-
361 pression drives increased association between Vav1 and Raf. This increased interaction
362 facilitates phosphorylation and activation of Raf by pre-bound Akt and/or CK2 at S621

363 or perhaps S259. Constitutively bound 14-3-3 may also stabilize the S621 phosphory-
364 lation, modulate the activity and/or up-regulate autophosphorylation. Activated Raf can
365 then drive ERK activation, which in turn closes the positive feedback loop by activating
366 Raf transcription factors e.g., Sp1 and/or STAT1 (47–50). We tested this working hy-
367 pothesis using mathematical modeling. The model recapitulated both ATRA time-course
368 data as well as the GW5074 inhibitor effects. This suggested the proposed Raf-Vav1
369 architecture was at least consistent with the experimental studies. Further, analysis of
370 the Raf-Vav1 model identified bistability in ppERK levels. Thus, two possible MAPK ac-
371 tivation branches were possible for experimentally testable ATRA values. The analysis
372 also suggested the ATRA-induced Raf-Vav1 architecture could be locked into a sustained
373 signaling mode (high ppERK) even in the absence of a ATRA signal. This locked-in prop-
374 erty could give rise to an ATRA-induction memory. We validated the treatment memory
375 property predicted by the Raf-Vav1 circuit experimentally using ATRA-washout experi-
376 ments. ERK phosphorylation levels remained high for more than 96 hr after ATRA was
377 removed. Previous studies demonstrated that HL-60 cells possessed an inheritable mem-
378 ory of ATRA stimulus (51). Although the active state was self-sustaining, the inactive state
379 demonstrated considerable robustness to perturbation. For example, we found that 50x
380 overexpression of Raf was required to reliably lock MAPK into the activated state, while
381 small perturbations had almost no effect on ppERK levels over the entire ensemble. CD38
382 expression correlated with the ppERK, suggesting its involvement in the signaling com-
383 plex. Our computational and experimental results showed that positive feedback, through
384 ERK-dependent Raf expression, could sustain MAPK signaling through many division cy-
385 cles. Such molecular mechanisms could underly aspects of cellular memory associated
386 to consecutive ATRA treatments.

387 There were several issues that can be explored further with the effective ATRA differ-
388 entiation model. First, there was likely missing connectivity in the effective differentiation

389 circuit. Decreasing BLR1 expression with simultaneously sustained cRaf-pS261 activa-
390 tion was not captured by the current network architecture. This suggested that signal-
391 some, once activated, had a long lifetime as decreased BLR1 expression did not impact
392 cRaf-pS261 abundance. We could model this by separating signalsome formation into an
393 inactive precursor pool that is transformed to a long-lived activated signalsome by MAPK
394 activation. We should also explore adding additional downstream biological modules to
395 this skeleton model, for example the upregulation of reactive oxygen markers such as
396 p47Phox or cell cycle arrest components to capture the switch from an actively prolifer-
397 ating population to a population in G0-arrest. Next, the choice of max/min integration
398 rules or the particular form of the transfer functions could also be explored. Integration
399 rules other than max/min could be used, such as the mean or the product, assuming the
400 range of the transfer functions is always $f \in [0, 1]$. Alternative integration rules might
401 have different properties which could influence model identification or performance. For
402 example, a mean integration rule would be differentiable, allowing derivative-based opti-
403 mization approaches to be used. The form of the transfer function could also be explored.
404 We choose hill-like functions because of their prominence in the systems and synthetic
405 biology community. However, many other transfer functions are possible.

406 **Materials and Methods**

407 *Effective gene expression model equations.* We decomposed the ATRA-induced differ-
 408 entiation program into three modules; a signal initiation module that sensed and trans-
 409 formed the ATRA signal into activated cRaf-pS621 and the ATRA-RXR/RAR (activated
 410 Trigger) signals; a signal integration module that controlled the expression of upstream
 411 transcription factors given cRaf-pS621 and activated Trigger signals; and a phenotype
 412 module which encoded the expression of functional differentiation markers from the ATRA-
 413 inducible transcription factors. The output of the signal initiation module was the input to
 414 the gene expression model. For each gene $j = 1, 2, \dots, \mathcal{G}$, we modeled both the mRNA
 415 (m_j), protein (p_j) and signaling species abundance:

$$\frac{dm_j}{dt} = r_{T,j} - (\mu + \theta_{m,j}) m_j + \lambda_j \quad (1)$$

$$\frac{dp_j}{dt} = r_{X,j} - (\mu + \theta_{p,j}) p_j \quad (2)$$

$$g(p_1, \dots, p_{\mathcal{G}}, \kappa) = 0 \quad (3)$$

416 The terms $r_{T,j}$ and $r_{X,j}$ denote the specific rates of transcription, and translation while
 417 the terms $\theta_{m,j}$ and $\theta_{p,j}$ denote first-order degradation constants for mRNA and protein,
 418 respectively. The specific transcription rate $r_{T,j}$ was modeled as the product of a kinetic
 419 term $\bar{r}_{T,j}$ and a control term u_j which described how the abundance of transcription fac-
 420 tors, or other regulators influenced the expression of gene j . The kinetic transcription
 421 term $\bar{r}_{T,j}$ was modeled as:

$$\bar{r}_{T,j} = V_T^{max} \left(\frac{L_{T,o}}{L_{T,j}} \right) \left(\frac{G_j}{K_T + G_j} \right) \quad (4)$$

422 where the maximum gene expression rate V_T^{max} was defined as the product of a char-
 423 acteristic transcription rate constant (k_T) and the abundance of RNA polymerase (R_1),

424 $V_T^{max} = k_T(R_1)$. The $(L_{T,o}/L_{T,j})$ term denotes the ratio of transcription read lengths; $L_{T,o}$
 425 represents a characteristic gene length, while $L_{T,j}$ denotes the length of gene j . Thus,
 426 the ratio $(L_{T,o}/L_{T,j})$ is a gene specific correction to the characteristic transcription rate
 427 V_T^{max} . The degradation rate constants were defined as $\theta_{m,j}$ and $\theta_{p,j}$ denote characteristic
 428 degradation constants for mRNA and protein, respectively. Lastly, the λ_j term denotes the
 429 constitutive rate of expression of gene j .

430 The gene expression control term $0 \leq u_j \leq 1$ depended upon the combination of fac-
 431 tors which influenced the expression of gene j . If the expression of gene j was influenced
 432 by $1, \dots, m$ factors, we modeled this relationship as $u_j = \mathcal{I}_j(f_{1j}(\cdot), \dots, f_{mj}(\cdot))$ where
 433 $0 \leq f_{ij}(\cdot) \leq 1$ denotes a regulatory transfer function quantifying the influence of factor i
 434 on the expression of gene j , and $\mathcal{I}_j(\cdot)$ denotes an integration rule which combines the
 435 individual regulatory inputs for gene j into a single control term. In this study, the integra-
 436 tion rule governing gene expression was the weighted fraction of promoter configurations
 437 that resulted in gene expression (52):

$$u_j = \frac{W_{R_{1,j}} + \sum_n W_{nj} f_{nj}}{1 + W_{R_{1,j}} + \sum_d W_{dj} f_{dj}} \quad (5)$$

438 The numerator, the weighted sum (with weights W_{nj}) of promoter configurations leading to
 439 gene expression, was normalized by all possible promoter configurations. The likelihood
 440 of each configuration was quantified by the transfer function f_{nj} (which we modeled using
 441 hill like functions), while the lead term in the numerator $W_{R_{1,j}}$ denotes the weight of con-
 442 stitutive expression for gene j . Given this formulation, the rate of constitutive expression
 443 was then given by:

$$\lambda_j = \bar{r}_{T,j} \left(\frac{W_{R_{1,j}}}{1 + W_{R_{1,j}}} \right) \quad (6)$$

444 If a gene expression process had no modifying factors, $u_j = 1$. Lastly, the specific trans-

445 lation rate was modeled as:

$$r_{X,j} = V_X^{\max} \left(\frac{L_{X,o}}{L_{X,j}} \right) \left(\frac{m_j}{K_X + m_j} \right) \quad (7)$$

446 where V_X^{\max} denotes a characteristic maximum translation rate estimated from literature,
447 and K_X denotes a translation saturation constant. The characteristic maximum translation
448 rate was defined as the product of a characteristic translation rate constant (k_X) and
449 the Ribosome abundance (R_2), $V_X^{\max} = k_X (R_2)$. As was the case for transcription, we
450 corrected the characteristic translation rate by the ratio of the length of a characteristic
451 transcription normalized by the length of transcript j .

452 *Signaling model equations.* The signal initiation, and integration modules required the
453 abundance of cRaf-pS621 and ATRA-RXR/RAR (activated Trigger) as inputs. However,
454 our base model described only the abundance of inactive proteins e.g., cRaf or RXR/RAR
455 but not the activated forms. To address this issue, we estimated pseudo steady state
456 approximations for the abundance of cRaf-pS621 and activated Trigger (shown generally
457 as Eq (3)). The abundance of activated trigger ($x_{a,1}$) was estimated directly from the
458 RXR/RAR abundance ($x_{u,1}$):

$$x_{a,1} \sim x_{u,1} \left(\frac{\alpha \cdot \text{ATRA}}{1 + \alpha \cdot \text{ATRA}} \right) \quad (8)$$

459 where α denotes a gain parameter; $\alpha = 0.0$ if ATRA is less than a threshold, and $\alpha = 0.1$
460 if ATRA is greater than the differentiation threshold. The abundance of cRaf-pS621 was
461 estimated by making the pseudo steady state approximation on the cRaf-pS621 balance.
462 The abundance of an activated signaling species i was given by:

$$\frac{dx_i}{dt} = r_{+,i}(\mathbf{x}, \mathbf{k}) - (\mu + k_{d,i}) x_i \quad i = 1, \dots, \mathcal{M} \quad (9)$$

463 The quantity x_i denotes concentration of signaling species i , while \mathcal{R} and \mathcal{M} denote
 464 the number of signaling reactions and signaling species in the model, respectively. The
 465 term $r_{+,i}(\mathbf{x}, \mathbf{k})$ denotes the rate of generation of activated species i , while μ denotes
 466 the specific growth rate, and $k_{d,i}$ denotes the rate constant controlling the non-specific
 467 degradation of x_i . We neglected deactivation reactions e.g., phosphatase activities. We
 468 assumed that signaling processes were fast compared to gene expression; this allowed
 469 us to approximate the signaling balance as:

$$x_i^* \simeq \frac{r_{+,i}(\mathbf{x}, \mathbf{k})}{(\mu + k_{d,i})} \quad i = 1, \dots, \mathcal{M} \quad (10)$$

470 The generation rate was written as the product of a kinetic term ($\bar{r}_{+,i}$) and a control term
 471 (v_i). The control terms $0 \leq v_j \leq 1$ depended upon the combination of factors which in-
 472 fluenced rate process j . If rate j was influenced by $1, \dots, m$ factors, we modeled this
 473 relationship as $v_j = \mathcal{I}_j(f_{1j}(\cdot), \dots, f_{mj}(\cdot))$ where $0 \leq f_{ij}(\cdot) \leq 1$ denotes a regulatory
 474 transfer function quantifying the influence of factor i on rate j . The function $\mathcal{I}_j(\cdot)$ is an
 475 integration rule which maps the output of regulatory transfer functions into a control vari-
 476 able. In this study, we used $\mathcal{I}_j \in \{\min, \max\}$ and hill transfer functions (53). If a process
 477 had no modifying factors, $v_j = 1$. The kinetic rate of cRaf-pS621 generation $\bar{r}_{+,cRaf}$ was
 478 modeled as:

$$\bar{r}_{+,cRaf} = k_{+,cRaf} x_s \left(\frac{x_{cRaf}}{K_{+,cRaf} + x_{cRaf}} \right) \quad (11)$$

479 where x_s denotes the signalsome abundance, and $K_{+,cRaf}$ denotes a saturation constant
 480 governing cRaf-pS621 formation. The formation of cRaf-pS621 was regulated by only a
 481 single factor, the abundance of MAPK inhibitor, thus $v_{+,cRaf}$ took the form:

$$v_{+,cRaf} = \left(1 - \frac{I}{K_D + I} \right) \quad (12)$$

482 where I denotes the abundance of the MAPK inhibitor, and K_D denotes the inhibitor
483 affinity.

484 *Estimation of gene expression model parameters.* We estimated parameters appearing
485 in the mRNA and protein balances, the abundance of polymerases and ribosomes, tran-
486 scription and translation rates, the half-life of a typical mRNA and protein, and typical
487 values for the copies per cell of RNA polymerase and ribosomes from literature (Table 2).
488 The saturation constants K_X and K_T were adjusted so that gene expression and trans-
489 lation resulted in gene products on a biologically realistic concentration scale. Lastly, we
490 calculated the concentration for gene G_j by assuming, on average, that a cell had two
491 copies of each gene at any given time. Thus, the bulk of our gene expression model pa-
492 rameters were based directly upon literature values, and were not adjusted during model
493 identification. However, the remaining parameters, e.g., the W_{ij} appearing in the gene
494 expression control laws, or parameters appearing in the transfer functions f_{dij} , were esti-
495 mated from the protein expression and signaling data sets discussed here.

496 Signaling and gene expression model parameters were estimated by minimizing the
497 squared difference between simulations and experimental protein data set j . We mea-
498 sured the squared difference in the scale, fold change and shape for protein j :

$$E_j(\mathbf{k}) = \left(\mathcal{M}_j(t_-) - \hat{y}_j(t_-, \mathbf{k}) \right)^2 + \sum_{i=1}^{\mathcal{T}_j} \left(\hat{\mathcal{M}}_{ij} - \hat{y}_{ij}(\mathbf{k}) \right)^2 + \sum_{i=1}^{\mathcal{T}_j} \left(\mathcal{M}'_{ij} - y'_{ij}(\mathbf{k}) \right)^2 \quad (13)$$

499 The first term in Eqn. (13) quantified the initial *scale* error, directly before the addition
500 of ATRA. In this case, $\mathcal{M}_j(t_-)$ (the approximate concentration of protein j before the
501 addition of ATRA) was estimated from literature. This term was required because the
502 protein measurements were reported as the fold-change; thus, the data was normalized
503 by a control value measured before the addition of ATRA. However, the model operated on
504 a physical scale. The first term allowed the model to capture physically realistic changes

following ATRA addition. The second term quantified the difference in the *fold-change* of protein j as a function of time. The terms $\hat{\mathcal{M}}_{ij}$ and \hat{y}_{ij} denote the scaled experimental observations and simulation outputs (fold-change; protein normalized by control value directly before ATRA addition) at time i from protein j , where T_j denoted the number of time points for data set j . Lastly, the third term of the objective function measured the difference in the *shape* of the measured and simulated protein levels. The scaled value $0 \leq \mathcal{M}'_{ij} \leq 1$ was given by:

$$\hat{\mathcal{M}}_{ij} = \left(\mathcal{M}_{ij} - \min_i \mathcal{M}_{ij} \right) / \left(\max_i \mathcal{M}_{ij} - \min_i \mathcal{M}_{ij} \right) \quad (14)$$

where $\mathcal{M}'_{ij} = 0$ and $\mathcal{M}'_{ij} = 1$ describe the lowest (highest) intensity bands. A similar scaling was used for the simulation output. We minimized the total model residual $\sum_j E_j$ using a heuristic direct-search optimization procedure, subject to box constraints on the parameter values, starting from a random initial parameter guess. Each downhill step was archived and used for ensemble calculations. The optimization procedure (a covariance matrix adaptation evolution strategy) has been reported previously (54).

Estimation of an effective cell cycle arrest model. We formulated an effective N-order polynomial model of the fraction of cells undergoing ATRA-induced cell cycle arrest at time t , $\hat{\mathcal{A}}(t)$, as:

$$\hat{\mathcal{A}}(t) \simeq a_0 + \sum_{i=1}^{N-1} a_i \phi_i(\mathbf{p}(t), t) \quad (15)$$

where a_i were unknown parameters, and $\phi_i(\mathbf{p}(t), t)$ denotes a basis function. The basis functions were dependent upon the system state; in this study, we assumed $N = 4$ and basis functions of the form:

$$\phi_i(\mathbf{p}(t), t) = \left(\frac{t}{T} + \frac{p21}{E2F} \Big|_t \right)^{(i-1)} \quad (16)$$

524 The parameters a_0, \dots, a_3 were estimated directly from cell-cycle measurements (biologi-
525 cal replicates) using least-squares.

526 *Availability of model code.* The signaling and gene expression model equations, and the
527 parameter estimation procedure, were implemented in the Julia programming language.
528 The model equations were solved using the ODE23s routine of the ODE package (55). The
529 model code and parameter ensemble is freely available under an MIT software license
530 and can be downloaded from <http://www.varnerlab.org>.

531 *Cell culture and treatment* Human myeloblastic leukemia cells (HL-60 cells) were grown
532 in a humidified atmosphere of 5% CO₂ at 37°C and maintained in RPMI 1640 from Gibco
533 (Carlsbad, CA) supplemented with 5% heat inactivated fetal bovine serum from Hyclone
534 (Logan, UT) and 1× antibiotic/antimicotic (Gibco, Carlsbad, CA). Cells were cultured in
535 constant exponential growth (56). Experimental cultures were initiated at 0.1×10^6 cells/mL
536 24 hr prior to ATRA treatment; if indicated, cells were also treated with GW5074 (2 μ M) 18
537 hr before ATRA treatment. For the cell culture washout experiments, cells were treated
538 with ATRA for 24 hr, washed 3x with prewarmed serum supplemented culture medium
539 to remove ATRA, and reseeded in ATRA-free media as described. Western blot analysis
540 was performed at incremental time points after removal of ATRA.

541 *Chemicals* All-Trans Retinoic Acid (ATRA) from Sigma-Aldrich (St. Louis, MO) was dis-
542 solved in 100% ethanol with a stock concentration of 5mM, and used at a final concen-
543 tration of 1 μ M (unless otherwise noted). The cRaf inhibitor GW5074 from Sigma-Aldrich
544 (St. Louis, MO) was dissolved in DMSO with a stock concentration of 10mM, and used
545 at a final concentration of 2 μ M. HL-60 cells were treated with 2 μ M GW5074 with or with-
546 out ATRA (1 μ M) at 0 hr. This GW5074 dosage had a negligible effect on the cell cycle
547 distribution, compared to ATRA treatment alone.

548 *Immunoprecipitation and western blotting* Approximately 1.2×10^7 cells were lysed using
549 $400\mu\text{L}$ of M-Per lysis buffer from Thermo Scientific (Waltham, MA). Lysates were cleared
550 by centrifugation at $16,950 \times g$ in a micro-centrifuge for 20 min at 4°C . Lysates were
551 pre-cleared using $100\mu\text{L}$ protein A/G Plus agarose beads from Santa Cruz Biotechnology
552 (Santa Cruz, CA) by inverting overnight at 4°C . Beads were cleared by centrifugation and
553 total protein concentration was determined by a BCA assay (Thermo Scientific, Waltham,
554 MA). Immunoprecipitations were setup by bringing lysate to a concentration of 1g/L in a
555 total volume of $300\mu\text{L}$ (M-Per buffer was used for dilution). The anti-Raf antibody was
556 added at $3\mu\text{L}$. A negative control with no bait protein was also used to exclude the di-
557 rect interaction of proteins with the A/G beads. After 1 hr of inversion at 4°C , $20\mu\text{L}$ of
558 agarose beads was added and samples were left to invert overnight at 4°C . Samples
559 were then washed three times with M-Per buffer by centrifugation. Finally proteins were
560 eluted from agarose beads using a laemmli loading buffer. Eluted proteins were resolved
561 by SDS-PAGE and Western blotting. Total lysate samples were normalized by total protein
562 concentration ($20\mu\text{g}$ per sample) and resolved by SDS-PAGE and Western blotting. Sec-
563 ondary HRP bound antibody was used for visualization. All antibodies were purchased
564 from Cell Signaling (Boston, MA) with the exception of α -p621 Raf which was purchased
565 from Biosource/Invitrogen (Carlsbad, CA), and α -CK2 from BD Biosciences (San Jose,
566 CA).

567 *Morphology assessment* Untreated and ATRA-treated HL-60 cells were collected after
568 72 hr and cytocentrifuged for 3 min at 700 rpm onto glass slides. Slides were air-dried
569 and stained with Wright's stain. Slide images were captured at 40X (Leica DM LB 100T
570 microscope, Leica Microsystems).

571 **Competing interests**

572 The authors declare that they have no competing interests.

573 **Author's contributions**

574 J.V and A.Y directed the study. R.T, H.J, R.B and J.C conducted the cell culture measure-
575 ments. J.V, R.B, W.D, K.R and A.S developed the reduced order HL-60 models and the
576 parameter ensemble. W.D and J.V analyzed the model ensemble, and generated figures
577 for the manuscript. The manuscript was prepared and edited for publication by W.D, A.Y
578 and J.V.

579 **Acknowledgements**

580 We gratefully acknowledge the suggestions from the anonymous reviewers to improve
581 this manuscript.

582 **Funding**

583 We acknowledge the financial support to J.V. by the National Science Foundation CA-
584 REER (CBET-0846876) for the support of R.T. and H.J. In addition, we acknowledge
585 support to A.Y. from the National Institutes of Health (CA 30555, CA152870) and a grant
586 from New York State Stem Cell Science. Lastly, we acknowledge the financial support to
587 J.V. and A.Y. from the National Cancer Institute (#U54 CA143876). The content is solely
588 the responsibility of the authors and does not necessarily represent the official views of
589 the National Cancer Institute or the National Institutes of Health.

590 **References**

- 591 1. Bushue N, Wan YJY (2010) Retinoid pathway and cancer therapeutics. *Adv Drug*
592 *Deliv Rev* 62: 1285-98.
- 593 2. Tang XH, Gudas LJ (2011) Retinoids, retinoic acid receptors, and cancer. *Annu Rev*
594 *Pathol* 6: 345-64.
- 595 3. Cheung FSG, Lovicu FJ, Reichardt JKV (2012) Current progress in using vitamin d
596 and its analogs for cancer prevention and treatment. *Expert Rev Anticancer Ther*
597 12: 811-37.
- 598 4. Nilsson B (1984) Probable in vivo induction of differentiation by retinoic acid of
599 promyelocytes in acute promyelocytic leukaemia. *Br J Haematol* 57: 365-71.
- 600 5. Warrell RP Jr (1993) Retinoid resistance in acute promyelocytic leukemia: new
601 mechanisms, strategies, and implications. *Blood* 82: 1949-53.
- 602 6. Freemantle SJ, Spinella MJ, Dmitrovsky E (2003) Retinoids in cancer therapy and
603 chemoprevention: promise meets resistance. *Oncogene* 22: 7305-15.
- 604 7. Breitman TR, Selonick SE, Collins SJ (1980) Induction of differentiation of the hu-
605 man promyelocytic leukemia cell line (HL-60) by retinoic acid. *Proc Natl Acad Sci U*
606 *S A* 77: 2936–2940.
- 607 8. Yen A, Roberson MS, Varvayanis S, Lee AT (1998) Retinoic acid induced
608 mitogen-activated protein (MAP)/extracellular signal-regulated kinase (ERK) kinase-
609 dependent MAP kinase activation needed to elicit HL-60 cell differentiation and
610 growth arrest. *Cancer Res* 58: 3163–3172.
- 611 9. Hong HY, Varvayanis S, Yen A (2001) Retinoic acid causes MEK-dependent RAF
612 phosphorylation through RARalpha plus RXR activation in HL-60 cells. *Differentia-*
613 *tion* 68: 55–66.
- 614 10. Mangelsdorf DJ, Ong ES, Dyck JA, Evans RM (1990) Nuclear receptor that identifies
615 a novel retinoic acid response pathway. *Nature* 345: 224–229.

- 616 11. Congleton J, MacDonald R, Yen A (2012) Src inhibitors, PP2 and dasatinib, increase
617 retinoic acid-induced association of Lyn and c-Raf (S259) and enhance MAPK-
618 dependent differentiation of myeloid leukemia cells. Leukemia 26: 1180-8.
- 619 12. Shen M, Bunaci R, Congleton J, Jensen H, Sayam L, et al. (2011) Interferon regu-
620 latory factor-1 binds c-Cbl, enhances mitogen activated protein kinase signaling and
621 promotes retinoic acid-induced differentiation of HL-60 human myelo-monoblastic
622 leukemia cells. Leuk Lymphoma 52: 2372-9.
- 623 13. Shen M, Yen A (2009) c-Cbl tyrosine kinase-binding domain mutant G306E abol-
624 ishes the interaction of c-Cbl with CD38 and fails to promote retinoic acid-induced
625 cell differentiation and G0 arrest. J Biol Chem 284: 25664–25677.
- 626 14. Yen A, Varvayanis S, Smith J, Lamkin T (2006) Retinoic acid induces expression of
627 SLP-76: expression with c-FMS enhances ERK activation and retinoic acid-induced
628 differentiation/G0 arrest of HL-60 cells. Eur J Cell Biol 85: 117–132.
- 629 15. Marchisio M, Bertagnolo V, Colamussi ML, Capitani S, Neri LM (1998) Phos-
630 phatidylinositol 3-kinase in HL-60 nuclei is bound to the nuclear matrix and increases
631 during granulocytic differentiation. Biochem Biophys Res Commun 253: 346-51.
- 632 16. Congleton J, Jiang H, Malavasi F, Lin H, Yen A (2011) ATRA-induced HL-60 myeloid
633 leukemia cell differentiation depends on the CD38 cytosolic tail needed for mem-
634 brane localization, but CD38 enzymatic activity is unnecessary. Exp Cell Res 317:
635 910–919.
- 636 17. Wang J, Yen A (2004) A novel retinoic acid-responsive element regulates retinoic
637 acid induced BLR1 expression. Mol Cell Biol 24: 2423 - 2443.
- 638 18. Yen A (1990) HL-60 cells as a model of growth and differentiation: the significance
639 of variant cells. Hematology Review 4: 5-46.
- 640 19. Yang T, Xiong Q, Enslen H, Davis R, Chow CW (2002) Phosphorylation of NFATc4
641 by p38 mitogen-activated protein kinases. Mol Cell Biol 22: 3892–3904.

- 642 20. Wang J, Yen A (2008) A MAPK-positive Feedback Mechanism for BLR1 Signaling
643 Propels Retinoic Acid-triggered Differentiation and Cell Cycle Arrest. *J Biol Chem*
644 283: 4375–4386.
- 645 21. Tasseff R, Nayak S, Song S, Yen A, Varner J (2011) Modeling and analysis of retinoic
646 acid induced differentiation of uncommitted precursor cells. *Integr Biol* 3: 578 - 591.
- 647 22. Jensen HA, Styskal LE, Tasseff R, Bunaciu RP, Congleton J, et al. (2013) The
648 src-family kinase inhibitor pp2 rescues inducible differentiation events in emergent
649 retinoic acid-resistant myeloblastic leukemia cells. *PLoS One* 8: e58621.
- 650 23. Jensen HA, Bunaciu RP, Ibabao CN, Myers R, Varner JD, et al. (2014) Retinoic acid
651 therapy resistance progresses from unilineage to bilineage in hl-60 leukemic blasts.
652 *PLoS One* 9: e98929.
- 653 24. Jensen HA, Bunaciu RP, Varner JD, Yen A (2015) Gw5074 and pp2 kinase inhibitors
654 implicate nontraditional c-raf and lyn function as drivers of retinoic acid-induced mat-
655 uration. *Cell Signal* 27: 1666-75.
- 656 25. Jensen HA, Yourish HB, Bunaciu RP, Varner JD, Yen A (2015) Induced myelomono-
657 cytic differentiation in leukemia cells is accompanied by noncanonical transcription
658 factor expression. *FEBS Open Bio* 5: 789-800.
- 659 26. Milo R, Jorgensen P, Moran U, Weber G, Springer M (2010) Bionumbers—the
660 database of key numbers in molecular and cell biology. *Nucleic Acids Res* 38: D750-
661 3.
- 662 27. Katagiri K, Hattori S, Nakamura S, Yamamoto T, Yoshida T, et al. (1994) Activation
663 of ras and formation of gap complex during tpa-induced monocytic differentiation of
664 hl-60 cells. *Blood* 84: 1780–1789.
- 665 28. Miranda MB, Johnson DE (2007) Signal transduction pathways that contribute to
666 myeloid differentiation. *Leukemia* 21: 1363–1377.
- 667 29. Hickstein DD, Back AL, Collins SJ (1989) Regulation of expression of the cd11b and

- 668 cd18 subunits of the neutrophil adherence receptor during human myeloid differen-
669 tiation. *J Biol Chem* 264: 21812–21817.
- 670 30. Hornstein I, Alcover A, Katzav S (2004) Vav proteins, masters of the world of cy-
671 toskeleton organization. *Cell Signal* 16: 1-11.
- 672 31. Ferrell J (2002) Self-perpetuating states in signal transduction: positive feedback,
673 double-negative feedback and bistability. *Curr Opin Cell Biol* 14: 140-8.
- 674 32. Laslo P, Spooner CJ, Warmflash A, Lancki DW, Lee HJ, et al. (2006) Multilineage
675 transcriptional priming and determination of alternate hematopoietic cell fates. *Cell*
676 126: 755-66.
- 677 33. Xiong W, Ferrell J (2003) A positive-feedback-based bistable 'memory module' that
678 governs a cell fate decision. *Nature* 426: 460-5.
- 679 34. Bagci EZ, Vodovotz Y, Billiar TR, Ermentrout GB, Bahar I (2006) Bistability in apop-
680 tosis: roles of bax, bcl-2, and mitochondrial permeability transition pores. *Biophys J*
681 90: 1546-59.
- 682 35. Luan D, Zai M, Varner JD (2007) Computationally derived points of fragility of a
683 human cascade are consistent with current therapeutic strategies. *PLoS Comput*
684 *Biol* 3: e142.
- 685 36. Friedman AD (2007) Transcriptional control of granulocyte and monocyte develop-
686 ment. *Oncogene* 26: 6816-28.
- 687 37. Dahl R, Walsh JC, Lancki D, Laslo P, Iyer SR, et al. (2003) Regulation of macrophage
688 and neutrophil cell fates by the PU.1:C/EBPalpha ratio and granulocyte colony-
689 stimulating factor. *Nat Immunol* 4: 1029-36.
- 690 38. El-Benna J, Dang PMC, Gougerot-Pocidalo MA, Marie JC, Braut-Boucher F (2009)
691 p47phox, the phagocyte nadph oxidase/nox2 organizer: structure, phosphorylation
692 and implication in diseases. *Exp Mol Med* 41: 217-25.
- 693 39. Cleghon V, Morrison DK (1994) Raf-1 interacts with fyn and src in a non-

- 694 phosphotyrosine-dependent manner. *J Biol Chem* 269: 17749–17755.
- 695 40. Zimmermann S, Moelling K (1999) Phosphorylation and regulation of raf by akt (pro-
696 tein kinase b). *Science* 286: 1741–1744.
- 697 41. Ritt DA, Zhou M, Conrads TP, Veenstra TD, Copeland TD, et al. (2007) Ck2 is a
698 component of the ksr1 scaffold complex that contributes to raf kinase activation.
699 *Curr Biol* 17: 179–184.
- 700 42. Hekman M, Wiese S, Metz R, Albert S, Troppmair J, et al. (2004) Dynamic changes
701 in c-raf phosphorylation and 14-3-3 protein binding in response to growth factor stim-
702 ulation: differential roles of 14-3-3 protein binding sites. *J Biol Chem* 279: 14074–
703 14086.
- 704 43. Dhillon AS, Yip YY, Grindlay GJ, Pakay JL, Dangers M, et al. (2009) The c-terminus
705 of raf-1 acts as a 14-3-3-dependent activation switch. *Cell Signal* 21: 1645–1651.
- 706 44. Song JS, Gomez J, Stancato LF, Rivera J (1996) Association of a p95 vav-containing
707 signaling complex with the fcepsilonri gamma chain in the rbl-2h3 mast cell line.
708 evidence for a constitutive in vivo association of vav with grb2, raf-1, and erk2 in an
709 active complex. *J Biol Chem* 271: 26962–26970.
- 710 45. Costello PS, Walters AE, Mee PJ, Turner M, Reynolds LF, et al. (1999) The rho-
711 family gtp exchange factor vav is a critical transducer of t cell receptor signals to the
712 calcium, erk, and nf-kappab pathways. *Proc Natl Acad Sci U S A* 96: 3035–3040.
- 713 46. Graham D, Robertson C, Bautista J, Mascarenhas F, Diacovo M, et al. (2007)
714 Neutrophil-mediated oxidative burst and host defense are controlled by a Vav-
715 PLCgamma2 signaling axis in mice. *J Clin Invest* 117: 3445–3452.
- 716 47. Kim HS, Lim IK (2009) Phosphorylated extracellular signal-regulated protein kinases
717 1 and 2 phosphorylate sp1 on serine 59 and regulate cellular senescence via tran-
718 scription of p21sdi1/cip1/waf1. *J Biol Chem* 284: 15475–15486.
- 719 48. Milanini-Mongiat J, Pouys?gur J, Pag?e G (2002) Identification of two sp1 phos-

- 720 phosphorylation sites for p42/p44 mitogen-activated protein kinases: their implication in
721 vascular endothelial growth factor gene transcription. *J Biol Chem* 277: 20631–
722 20639.
- 723 49. Zhang Y, Cho YY, Petersen BL, Zhu F, Dong Z (2004) Evidence of stat1 phosphory-
724 lation modulated by mapks, mek1 and msk1. *Carcinogenesis* 25: 1165–1175.
- 725 50. Li Z, Theus MH, Wei L (2006) Role of erk 1/2 signaling in neuronal differentiation of
726 cultured embryonic stem cells. *Dev Growth Differ* 48: 513–523.
- 727 51. Yen A, Reece SL, Albright KL (1984) Dependence of hl-60 myeloid cell differentiation
728 on continuous and split retinoic acid exposures: precommitment memory associated
729 with altered nuclear structure. *J Cell Physiol* 118: 277–286.
- 730 52. Moon TS, Lou C, Tamsir A, Stanton BC, Voigt CA (2012) Genetic programs con-
731 structed from layered logic gates in single cells. *Nature* 491: 249-53.
- 732 53. Wayman JA, Sagar A, Varner JD (2015) Dynamic modeling of cell-free biochemical
733 networks using effective kinetic models. *Processes* 3: 138.
- 734 54. Igel C, Hansen N, Roth S (2007) Covariance matrix adaptation for multi-objective
735 optimization. *Evol Comput* 15: 1-28.
- 736 55. Bezanson J, Edelman A, Karpinski S, Shah VB (2014) Julia: A fresh approach to
737 numerical computing. *CoRR* abs/1411.1607.
- 738 56. Brooks SC, Kazmer S, Levin AA, Yen A (1996) Myeloid differentiation and retinoblas-
739 toma phosphorylation changes in HL-60 cells induced by retinoic acid receptor- and
740 retinoid X receptor-selective retinoic acid analogs. *Blood* 87: 227–237.
- 741 57. Rishi AK, Gerald TM, Shao ZM, Li XS, Baumann RG, et al. (1996) Regulation of the
742 human retinoic acid receptor alpha gene in the estrogen receptor negative human
743 breast carcinoma cell lines skbr-3 and mda-mb-435. *Cancer Res* 56: 5246-52.
- 744 58. Mueller BU, Pabst T, Fos J, Petkovic V, Fey MF, et al. (2006) Atra resolves the dif-
745 ferentiation block in t(15;17) acute myeloid leukemia by restoring pu.1 expression.

- 746 Blood 107: 3330-8.
- 747 59. Luo XM, Ross AC (2006) Retinoic acid exerts dual regulatory actions on the ex-
748 pression and nuclear localization of interferon regulatory factor-1. *Exp Biol Med*
749 (Maywood) 231: 619-31.
- 750 60. Sylvester I, Schöler HR (1994) Regulation of the oct-4 gene by nuclear receptors.
751 *Nucleic Acids Res* 22: 901-11.
- 752 61. Drach J, McQueen T, Engel H, Andreeff M, Robertson KA, et al. (1994) Retinoic
753 acid-induced expression of cd38 antigen in myeloid cells is mediated through
754 retinoic acid receptor-alpha. *Cancer Res* 54: 1746-52.
- 755 62. Liu M, Iavarone A, Freedman LP (1996) Transcriptional activation of the human
756 p21(waf1/cip1) gene by retinoic acid receptor. correlation with retinoid induction of
757 u937 cell differentiation. *J Biol Chem* 271: 31723-8.
- 758 63. Bunaciu RP, Yen A (2013) 6-formylindolo (3,2-b)carbazole (ficz) enhances retinoic
759 acid (ra)-induced differentiation of hl-60 myeloblastic leukemia cells. *Mol Cancer* 12:
760 39.
- 761 64. Balmer JE, Blomhoff R (2002) Gene expression regulation by retinoic acid. *J Lipid*
762 *Res* 43: 1773-808.
- 763 65. Rosen ED, Hsu CH, Wang X, Sakai S, Freeman MW, et al. (2002) C/ebpalpha in-
764 duces adipogenesis through ppargamma: a unified pathway. *Genes Dev* 16: 22-6.
- 765 66. Varley CL, Bacon EJ, Holder JC, Southgate J (2009) Foxa1 and irf-1 intermediary
766 transcriptional regulators of ppargamma-induced urothelial cytodifferentiation. *Cell*
767 *Death Differ* 16: 103-14.
- 768 67. Bruemmer D, Yin F, Liu J, Berger JP, Sakai T, et al. (2003) Regulation of the growth
769 arrest and dna damage-inducible gene 45 (gadd45) by peroxisome proliferator-
770 activated receptor gamma in vascular smooth muscle cells. *Circ Res* 93: e38-47.
- 771 68. Delerive P, De Bosscher K, Besnard S, Vanden Berghe W, Peters JM, et al. (1999)

- 772 PEROXISOME PROLIFERATOR-ACTIVATED RECEPTOR ALPHA NEGATIVELY REGULATES THE VASCULAR
773 INFLAMMATORY GENE RESPONSE BY NEGATIVE CROSS-TALK WITH TRANSCRIPTION FACTORS NF-
774 KAPPAB AND AP-1. J BIOL CHEM 274: 32048-54.
- 775 69. Altiok S, Xu M, Spiegelman BM (1997) Ppargamma induces cell cycle withdrawal:
776 inhibition of e2f/dp dna-binding activity via down-regulation of pp2a. GENES DEV 11:
777 1987-98.
- 778 70. Fei J, Cook C, Gillespie M, Yu B, Fullen K, et al. (2011) Atherogenic ω -6 lipids mod-
779 ulate ppar- egr-1 crosstalk in vascular cells. PPAR RES 2011: 753917.
- 780 71. Song EK, Lee YR, Kim YR, Yeom JH, Yoo CH, et al. (2012) Naadp mediates insulin-
781 stimulated glucose uptake and insulin sensitization by ppar γ in adipocytes. CELL REP
782 2: 1607-19.
- 783 72. Szanto A, Nagy L (2005) Retinoids potentiate peroxisome proliferator-activated re-
784 ceptor gamma action in differentiation, gene expression, and lipid metabolic pro-
785 cesses in developing myeloid cells. Mol Pharmacol 67: 1935-43.
- 786 73. Han S, Sidell N, Fisher PB, Roman J (2004) Up-regulation of p21 gene expres-
787 sion by peroxisome proliferator-activated receptor gamma in human lung carcinoma
788 cells. Clin Cancer Res 10: 1911-9.
- 789 74. Von Knethen A, Brüne B (2002) Activation of peroxisome proliferator-activated re-
790 ceptor gamma by nitric oxide in monocytes/macrophages down-regulates p47phox
791 and attenuates the respiratory burst. J Immunol 169: 2619-26.
- 792 75. Dispirito JR, Fang B, Wang F, Lazar MA (2013) Pruning of the adipocyte peroxisome
793 proliferator-activated receptor γ cistrome by hematopoietic master regulator pu.1.
794 Mol Cell Biol 33: 3354-64.
- 795 76. Chen H, Ray-Gallet D, Zhang P, Hetherington CJ, Gonzalez DA, et al. (1995) Pu.1
796 (spi-1) autoregulates its expression in myeloid cells. Oncogene 11: 1549-60.
- 797 77. Steidl U, Rosenbauer F, Verhaak RGW, Gu X, Ebralidze A, et al. (2006) Essential

- 798 role of jun family transcription factors in pu.1 knockdown-induced leukemic stem
799 cells. Nat Genet 38: 1269-77.
- 800 78. Pahl HL, Scheibe RJ, Zhang DE, Chen HM, Galson DL, et al. (1993) The proto-
801 oncogene pu.1 regulates expression of the myeloid-specific cd11b promoter. J Biol
802 Chem 268: 5014-20.
- 803 79. Yuki H, Ueno S, Tatetsu H, Niiro H, Iino T, et al. (2013) Pu.1 is a potent tumor
804 suppressor in classical hodgkin lymphoma cells. Blood 121: 962-70.
- 805 80. Li SL, Schlegel W, Valente AJ, Clark RA (1999) Critical flanking sequences of pu.1
806 binding sites in myeloid-specific promoters. J Biol Chem 274: 32453-60.
- 807 81. Timchenko N, Wilson DR, Taylor LR, Abdelsayed S, Wilde M, et al. (1995) Autoreg-
808 ulation of the human c/ebp alpha gene by stimulation of upstream stimulatory factor
809 binding. Mol Cell Biol 15: 1192-202.
- 810 82. Lidonnici MR, Audia A, Soliera AR, Prisco M, Ferrari-Amorotti G, et al. (2010) Ex-
811 pression of the transcriptional repressor gfi-1 is regulated by c/ebpalpha and is
812 involved in its proliferation and colony formation-inhibitory effects in p210bcr/abl-
813 expressing cells. Cancer Res 70: 7949-59.
- 814 83. D'Alo' F, Johansen LM, Nelson EA, Radomska HS, Evans EK, et al. (2003) The
815 amino terminal and e2f interaction domains are critical for c/ebp alpha-mediated
816 induction of granulopoietic development of hematopoietic cells. Blood 102: 3163-
817 71.
- 818 84. Pan Z, Hetherington CJ, Zhang DE (1999) Ccaat/enhancer-binding protein activates
819 the cd14 promoter and mediates transforming growth factor beta signaling in mono-
820 cyte development. J Biol Chem 274: 23242-8.
- 821 85. Harris TE, Albrecht JH, Nakanishi M, Darlington GJ (2001) Ccaat/enhancer-binding
822 protein-alpha cooperates with p21 to inhibit cyclin-dependent kinase-2 activity and
823 induces growth arrest independent of dna binding. J Biol Chem 276: 29200-9.

- 824 86. Bauvois B, Durant L, Laboureau J, Barthélémy E, Rouillard D, et al. (1999) Upreg-
825 ulation of cd38 gene expression in leukemic b cells by interferon types i and ii. *J*
826 *Interferon Cytokine Res* 19: 1059-66.
- 827 87. Passioura T, Dolnikov A, Shen S, Symonds G (2005) N-ras-induced growth suppres-
828 sion of myeloid cells is mediated by irf-1. *Cancer Res* 65: 797-804.
- 829 88. Dahl R, Iyer SR, Owens KS, Cuylear DD, Simon MC (2007) The transcriptional
830 repressor gfi-1 antagonizes pu.1 activity through protein-protein interaction. *J Biol*
831 *Chem* 282: 6473-83.
- 832 89. Duan Z, Horwitz M (2003) Targets of the transcriptional repressor oncoprotein gfi-1.
833 *Proc Natl Acad Sci U S A* 100: 5932-7.
- 834 90. Chen H, Zhang P, Radomska HS, Hetherington CJ, Zhang DE, et al. (1996) Octamer
835 binding factors and their coactivator can activate the murine pu.1 (spi-1) promoter.
836 *J Biol Chem* 271: 15743-52.
- 837 91. Behre G, Whitmarsh AJ, Coghlann MP, Hoang T, Carpenter CL, et al. (1999) c-jun
838 is a jnk-independent coactivator of the pu.1 transcription factor. *J Biol Chem* 274:
839 4939-46.
- 840 92. Kardassis D, Papakosta P, Pardali K, Moustakas A (1999) c-jun transactivates the
841 promoter of the human p21(waf1/cip1) gene by acting as a superactivator of the
842 ubiquitous transcription factor sp1. *J Biol Chem* 274: 29572-81.
- 843 93. Johnson DG, Ohtani K, Nevins JR (1994) Autoregulatory control of e2f1 expression
844 in response to positive and negative regulators of cell cycle progression. *Genes Dev*
845 8: 1514-25.
- 846 94. Fu M, Zhang J, Lin Y, Zhu X, Ehrengruber MU, et al. (2002) Early growth response
847 factor-1 is a critical transcriptional mediator of peroxisome proliferator-activated
848 receptor-gamma 1 gene expression in human aortic smooth muscle cells. *J Biol*
849 *Chem* 277: 26808-14.

- 850 95. Mak KS, Funnell APW, Pearson RCM, Crossley M (2011) Pu.1 and haematopoietic
851 cell fate: Dosage matters. *Int J Cell Biol* 2011: 808524.
- 852 96. Chen F, Wang Q, Wang X, Studzinski GP (2004) Up-regulation of egr1 by 1,25-
853 dihydroxyvitamin d3 contributes to increased expression of p35 activator of cyclin-
854 dependent kinase 5 and consequent onset of the terminal phase of hl60 cell differ-
855 entiation. *Cancer Res* 64: 5425-33.
- 856 97. Suh J, Jeon YJ, Kim HM, Kang JS, Kaminski NE, et al. (2002) Aryl hydrocarbon
857 receptor-dependent inhibition of ap-1 activity by 2,3,7,8-tetrachlorodibenzo-p-dioxin
858 in activated b cells. *Toxicol Appl Pharmacol* 181: 116-23.
- 859 98. Shen M, Bunaciu RP, Congleton J, Jensen HA, Sayam LG, et al. (2011) Inter-
860 feron regulatory factor-1 binds c-cbl, enhances mitogen activated protein kinase
861 signaling and promotes retinoic acid-induced differentiation of hl-60 human myelo-
862 monoblastic leukemia cells. *Leuk Lymphoma* 52: 2372-9.
- 863 99. Bunaciu RP, Yen A (2011) Activation of the aryl hydrocarbon receptor ahr promotes
864 retinoic acid-induced differentiation of myeloblastic leukemia cells by restricting ex-
865 pression of the stem cell transcription factor oct4. *Cancer Res* 71: 2371-80.
- 866 100. Jackson DA, Pombo A, Iborra F (2000) The balance sheet for transcription: an anal-
867 ysis of nuclear rna metabolism in mammalian cells. *FASEB J* 14: 242-54.
- 868 101. Zhao ZW, Roy R, Gebhardt JCM, Suter DM, Chapman AR, et al. (2014) Spatial orga-
869 nization of rna polymerase ii inside a mammalian cell nucleus revealed by reflected
870 light-sheet superresolution microscopy. *Proc Natl Acad Sci U S A* 111: 681-6.
- 871 102. Freitas R, Merkle R (2004) Kinematic Self-Replicating Machines. Oxford University
872 Press.
- 873 103. Yang E, van Nimwegen E, Zavolan M, Rajewsky N, Schroeder M, et al. (2003) De-
874 cay rates of human mrnas: correlation with functional characteristics and sequence
875 attributes. *Genome Res* 13: 1863-72.

- 876 104. Doherty MK, Hammond DE, Clague MJ, Gaskell SJ, Beynon RJ (2009) Turnover
877 of the human proteome: determination of protein intracellular stability by dynamic
878 silac. *J Proteome Res* 8: 104-12.
- 879 105. Sehgal PB, Derman E, Molloy GR, Tamm I, Darnell JE (1976) 5,6-dichloro-1-beta-
880 d-ribofuranosylbenzimidazole inhibits initiation of nuclear heterogeneous rna chains
881 in hela cells. *Science* 194: 431-3.
- 882 106. Darzacq X, Shav-Tal Y, de Turris V, Brody Y, Shenoy SM, et al. (2007) In vivo dy-
883 namics of rna polymerase ii transcription. *Nat Struct Mol Biol* 14: 796-806.
- 884 107. Kos M, Tollervey D (2010) Yeast pre-rrna processing and modification occur cotran-
885 scriptionally. *Mol Cell* 37: 809-20.
- 886 108. Darnell JE Jr (2013) Reflections on the history of pre-mrna processing and highlights
887 of current knowledge: a unified picture. *RNA* 19: 443-60.
- 888 109. Boström K, Wettsten M, Borén J, Bondjers G, Wiklund O, et al. (1986) Pulse-chase
889 studies of the synthesis and intracellular transport of apolipoprotein b-100 in hep g2
890 cells. *J Biol Chem* 261: 13800-6.
- 891 110. Meyers R, editor (2004) *Encyclopedia of Molecular Cell Biology and Molecular*
892 *Medicine*, Volume 1, 2nd Edition. ISBN: 978-3-527-30543-8. Wiley-Blackwell.
- 893 111. Rosenbluth MJ, Lam WA, Fletcher DA (2006) Force microscopy of nonadherent
894 cells: a comparison of leukemia cell deformability. *Biophys J* 90: 2994-3003.

Table 1: Myelomonocytic transcription factor connectivity used in the signal integration and phenotype modules.

Effector	Effect	Target	Source
RAR α	+	RAR α	(57)
	+	PU.1	(58)
	+	C/EBP α	(36)
	+	IRF-1	(59)
	-	Oct4	(60)
	+	CD38	(61)
	+	p21	(62)
	+	AhR	(63)
	+	Egr-1	(64)
PPAR γ	+	C/EBP α	(65)
	+	IRF-1	(66)
	+	Oct1	(67)
	-	AP-1	(68)
	-	E2F	(69)
	-	Egr-1	(70)
	+	CD38	(71)
	+	CD14	(72)
	+	p21	(73)
	-	p47Phox	(74)
PU.1	-	PPAR γ	(75)
	+	PU.1	(76)
	+	AP-1	(77)
	+	Egr-1	(32)
	+	CD11b	(78)
	+	p21	(79)
	+	p47Phox	(80)
C/EBP α	+	PPAR γ	(65)
	+	PU.1	(37)
	+	C/EBP α	(81)
	+	Gfi-1	(82)
	-	E2F	(83)
	+	CD14	(84)

896

	+	p21	(85)
IRF-1	+	CD38	(86)
	+	p21	(87)
	-	PU.1	(88)
	-	C/EBP α	(89)
	-	E2F	(89)
	-	Egr-1	(32)
	-	p21	(89)
Oct1	+	PU.1	(90)
AP-1	-	PPAR γ	(68)
	+	PU.1	(91)
	+	p21	(92)
E2F	+	E2F	(93)
Egr-1	+	PPAR γ	(94)
	-	Gfi-1	(95)
	+	CD14	(96)
AhR	+	AP-1	(97)
	+	IRF-1	(98)
	-	Oct4	(99)
	-	PU.1	

Table 2: Characteristic model parameters estimated from literature.

Symbol	Description	Value	Units	Source
R_1	RNA polymerase abundance	85,000	copies/cell	(100, 101)
R_2	Ribosome abundance	1×10^6	copies/cell	(102)
G_i	Characteristic gene abundance	2	copies/cell	this study
K_X	Saturation constant transcription	600	copies/cell	this study
K_T	Saturation constant translation	95,000	copies/cell	this study
$t_{1/2,m}$	characteristic mRNA half-life (transcription factor)	2-4	hr	(103)
$t_{1/2,p}$	characteristic protein half-life	10	hr	(104)
$\theta_{m,j}$	characteristic mRNA degradation constant	0.34	hr^{-1}	derived
$\theta_{p,j}$	characteristic protein degradation constant	0.07	hr^{-1}	derived
899				
t_d	HL-60 doubling time	19.5	hr	this study
μ	growth rate	0.035	hr^{-1}	derived
k_d	death rate	0.10μ	hr^{-1}	derived
e_T	elongation rate RNA polymerase	50-100	nt/s	(105–108)
e_X	elongation rate Ribosome	5	aa/s	(109)
$L_{T,o}$	characteristic gene length	15,000	nt	(110)
$L_{X,o}$	characteristic transcript length	5,000	nt	derived
k_T	characteristic transcription rate	1.44	hr^{-1}	derived
k_X	characteristic translation rate	3.60	hr^{-1}	derived
D	Diameter of an HL-60 cell	12.4	μm^3	(111)
f_C	cytoplasmic fraction	0.51	dimensionless	(111)

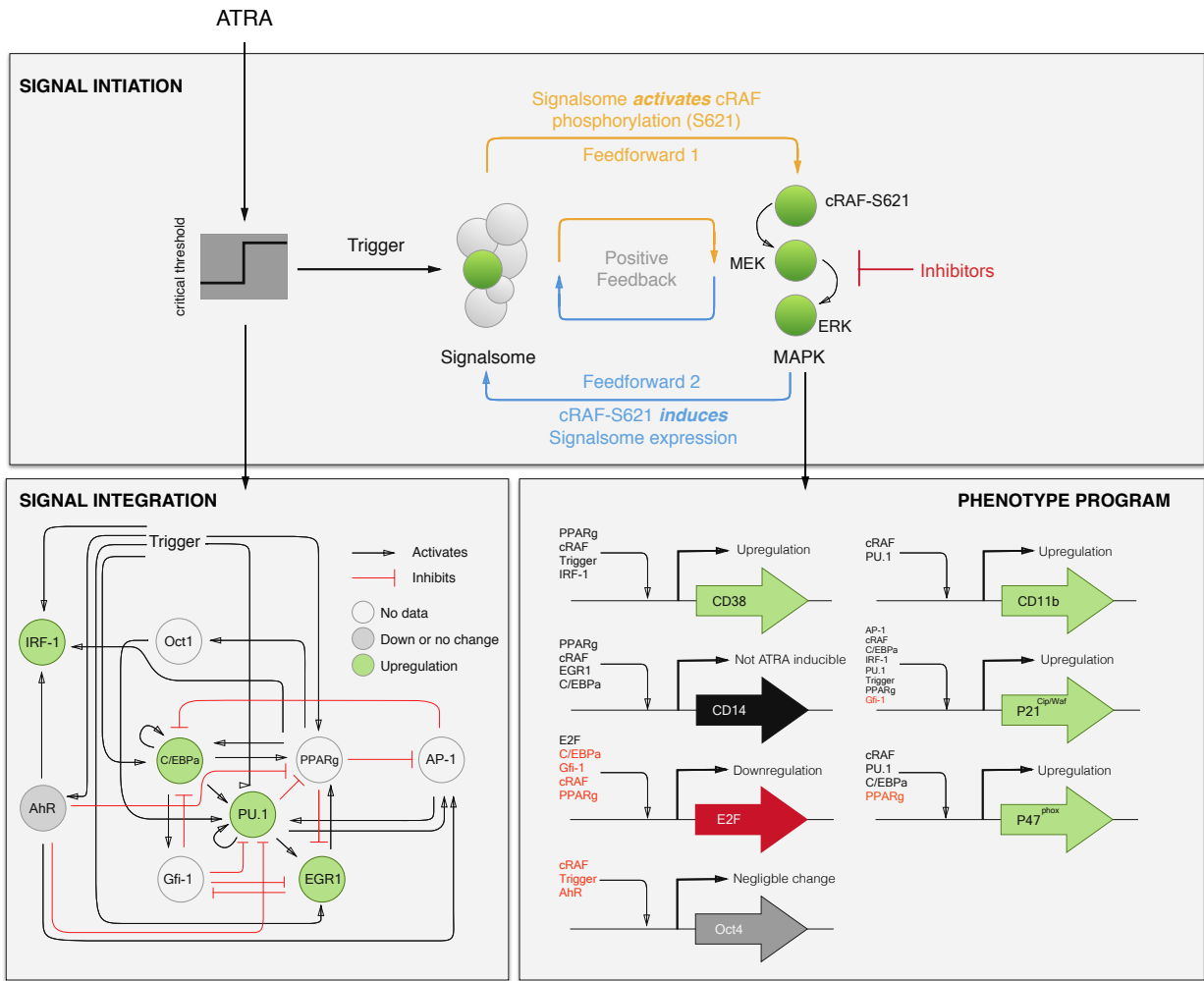


Fig. 1: Schematic of the effective ATRA differentiation circuit. Above a critical threshold, ATRA activates an upstream Trigger, which induces signalsome complex formation. Signalsome activates the mitogen-activated protein kinase (MAPK) cascade which in turn drives the differentiation program and signalsome formation. Both Trigger and activated cRaf-pS621 drive a phenotype gene expression program responsible for differentiation. Trigger activates the expression of a series of transcription factors which in combination with cRaf-pS621 result in phenotypic change.

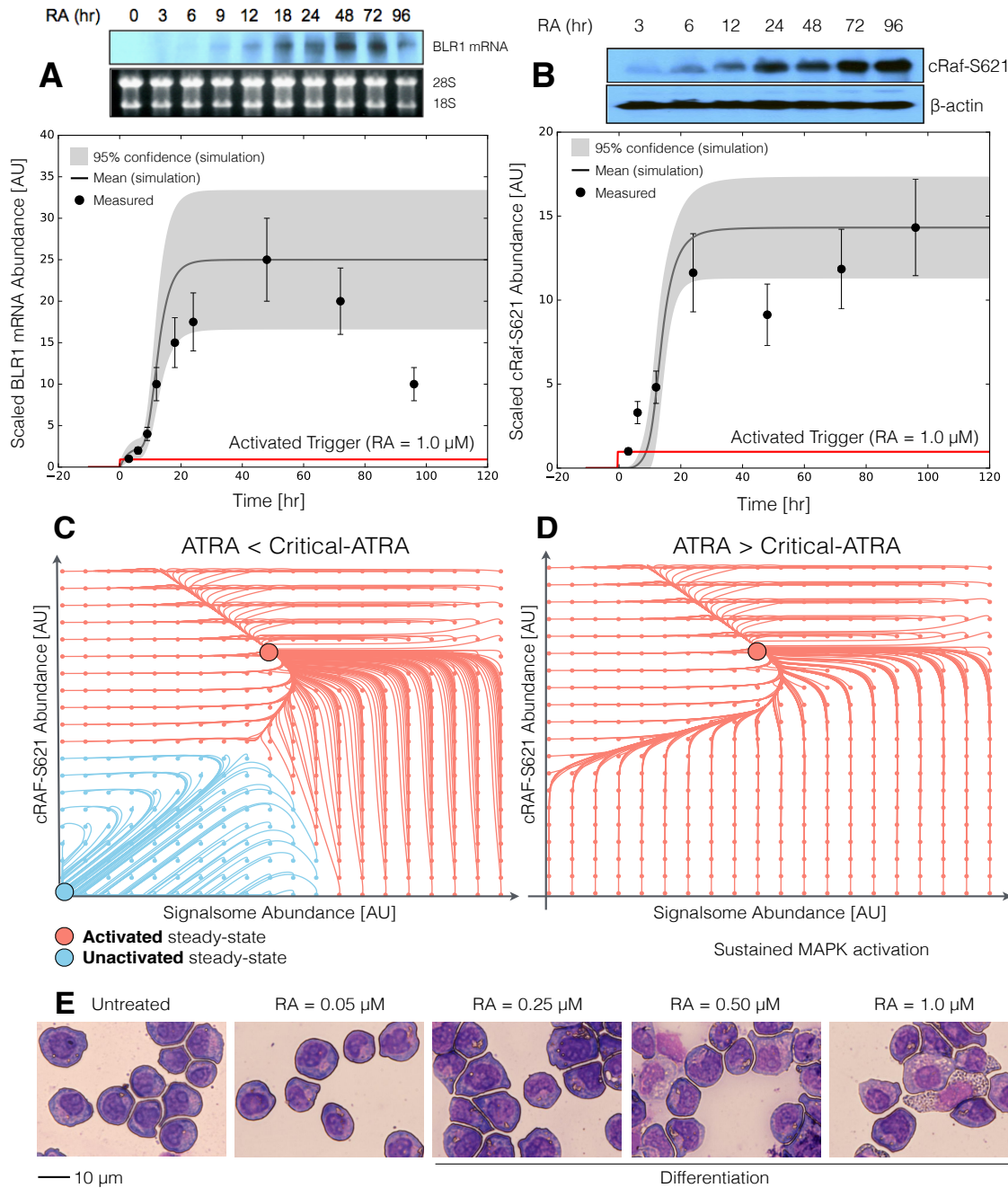


Fig. 2: Model analysis for ATRA-induced HL-60 differentiation. A: BLR1 mRNA versus time following exposure to 1 μ M ATRA at t = 0 hr. B: cRaf-pS621 versus time following exposure to 1 μ M ATRA at t = 0 hr. Points denote experimental measurements, solid lines denote the mean model performance. Shaded regions denote the 99% confidence interval calculated over the parameter ensemble. C: Signalsome and cRaf-pS621 nullclines for ATRA below the critical threshold. The model had two stable steady states and a single unstable state in this regime. D: Signalsome and cRaf-pS621 nullclines for ATRA above the critical threshold. In this regime the model had only a single stable steady state. E: Morphology of HL-60 as a function of ATRA concentration (t = 72 hr).

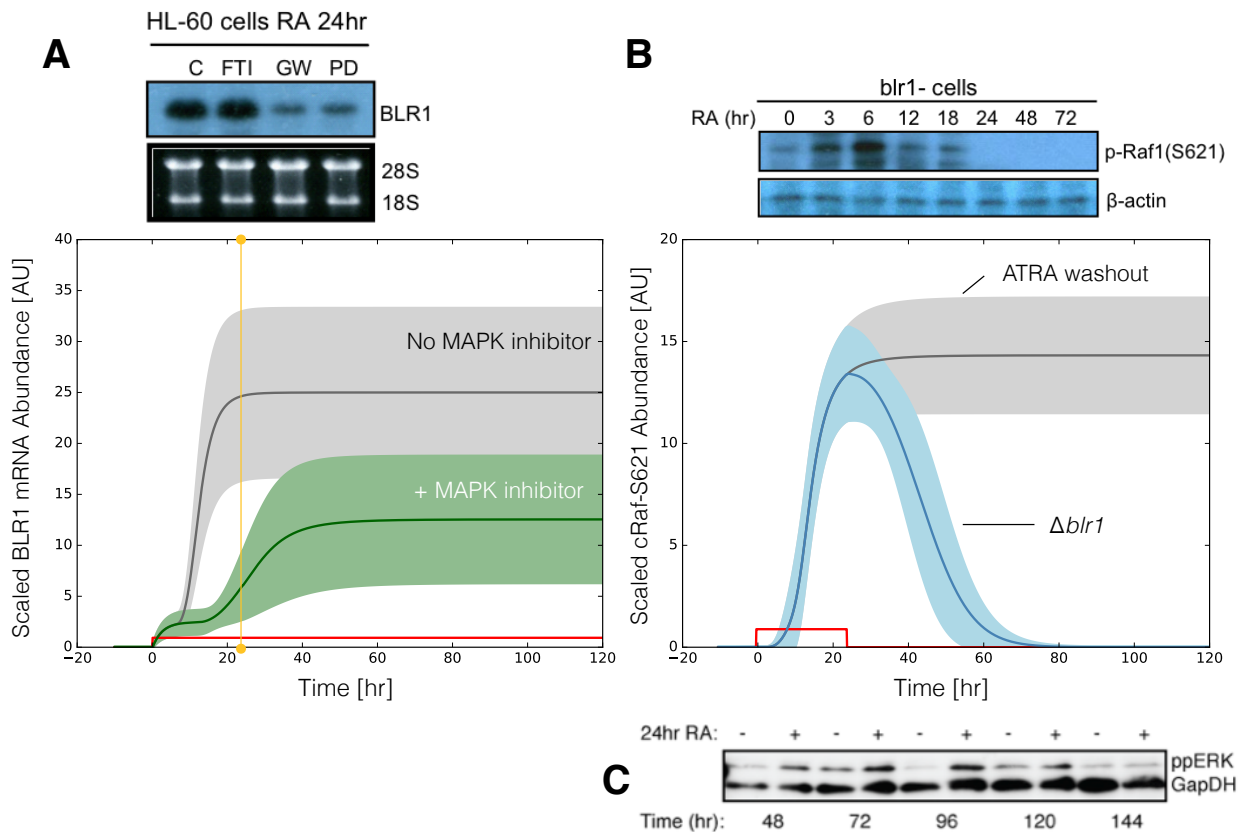


Fig. 3: Model simulation following exposure to $1\mu\text{M}$ ATRA. A: BLR1 mRNA versus time with and without MAPK inhibitor. B: cRaf-pS621 versus time following pulsed exposure to $1\mu\text{M}$ ATRA with and without BLR1. Solid lines denote the mean model performance, while shaded regions denote the 99% confidence interval calculated over the parameter ensemble. C: Western blot analysis of phosphorylated ERK1/2 in ATRA washout experiments. Experimental data in panels A and B were reproduced from Wang and Yen (20), data in panel C is reported in this study.

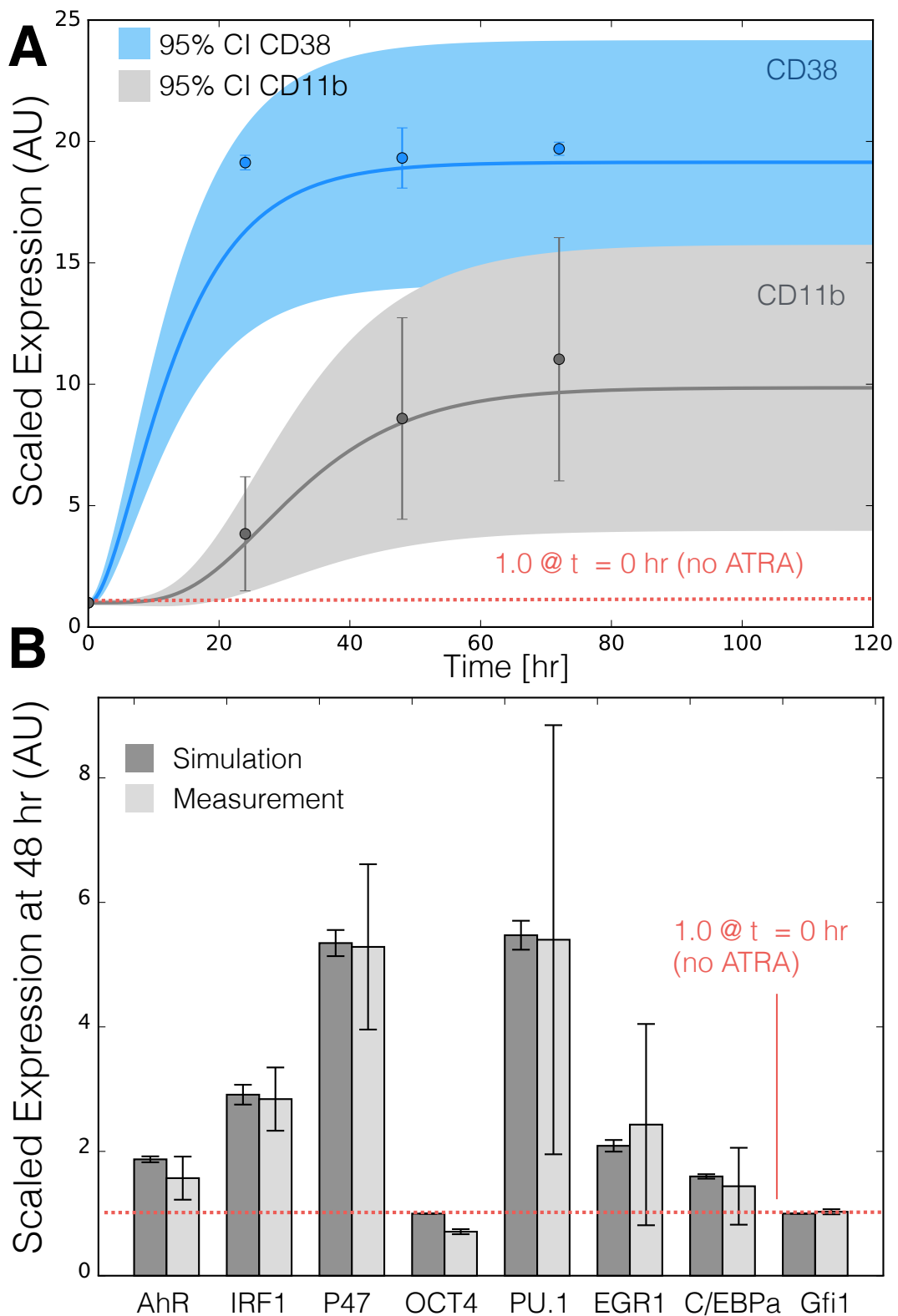


Fig. 4: Model simulation of the HL-60 gene expression program following exposure to $1\mu\text{M}$ ATRA at $t = 0$ hr. A: CD38 and CD11b expression versus time following ATRA exposure at time $t = 0$ hr. B: Gene expression at $t = 48$ hr following ATRA exposure. Experimental data in panels A and B were reproduced from Jensen et al. (25).

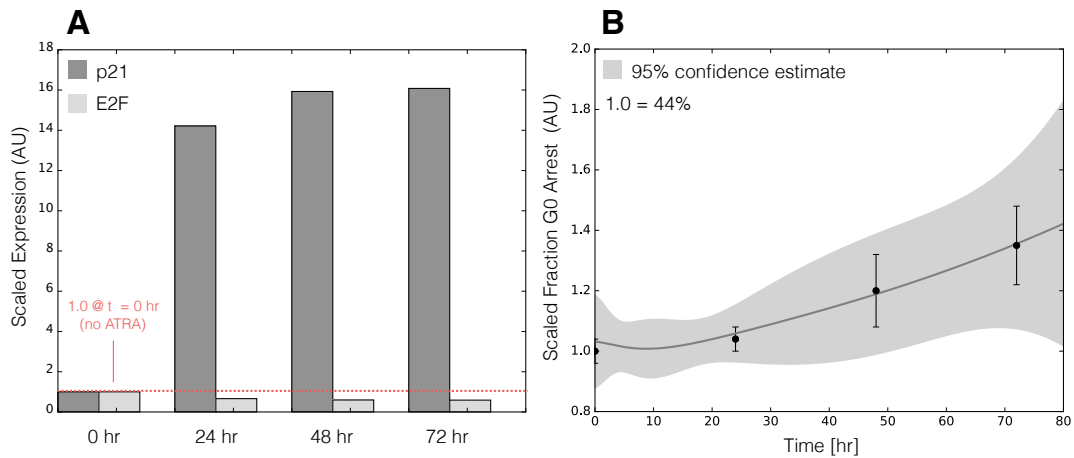


Fig. 5: Model simulation of HL-60 cell-cycle arrest following exposure to $1\mu\text{M}$ ATRA at $t = 0$ hr. A: Predicted p21 and E2F expression levels for the best parameter set following ATRA exposure at time $t = 0$ hr. B: Estimated fraction of HL-60 cells in G0 arrest following ATRA exposure at time $t = 0$ hr. The gray region denotes the 95% confidence estimate of the polynomial model. Experimental data in panel B was reproduced from Jensen et al. (25).

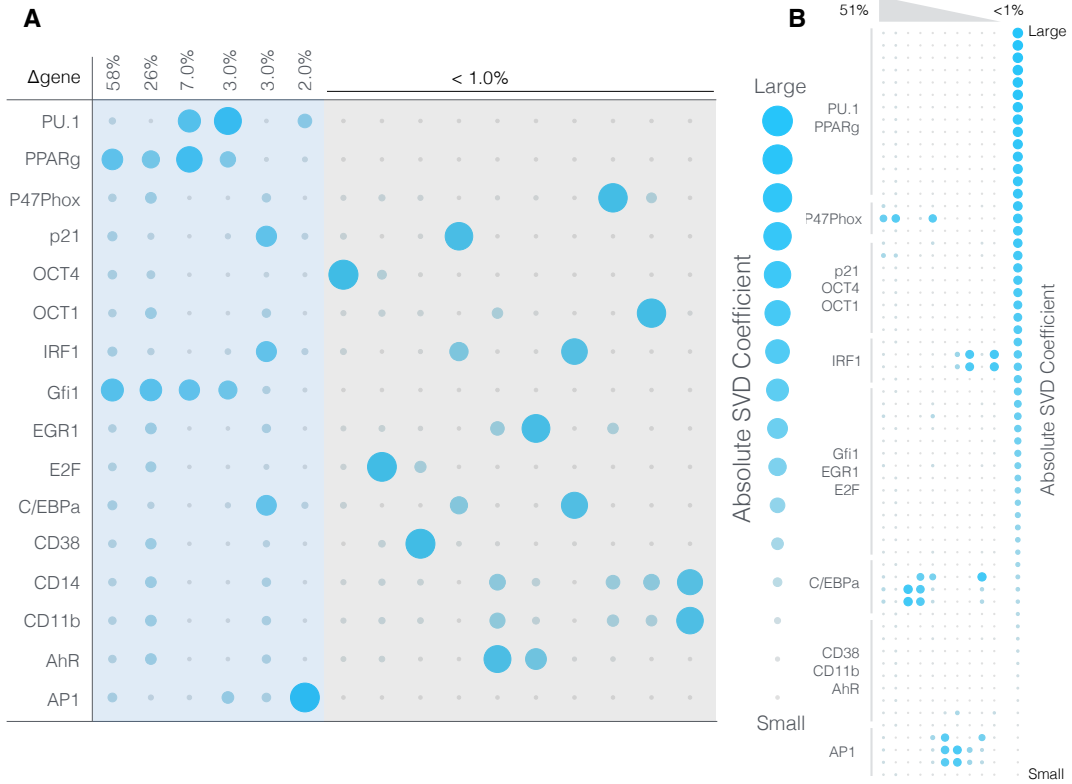


Fig. 6: Robustness of the HL-60 differentiation program following exposure to $1\mu\text{M}$ ATRA at $t = 0$ hr. A: Singular value decomposition of the system response (l^2 -norm between the perturbed and nominal state) following pairwise gene knockout simulations using the best fit parameter set. The percentage at the top of each column describes the fraction of the variance in the system state captured by the node combinations in the rows. B: Singular value decomposition of the system response (l^2 -norm between the perturbed and nominal state) following the pairwise removal of connections.

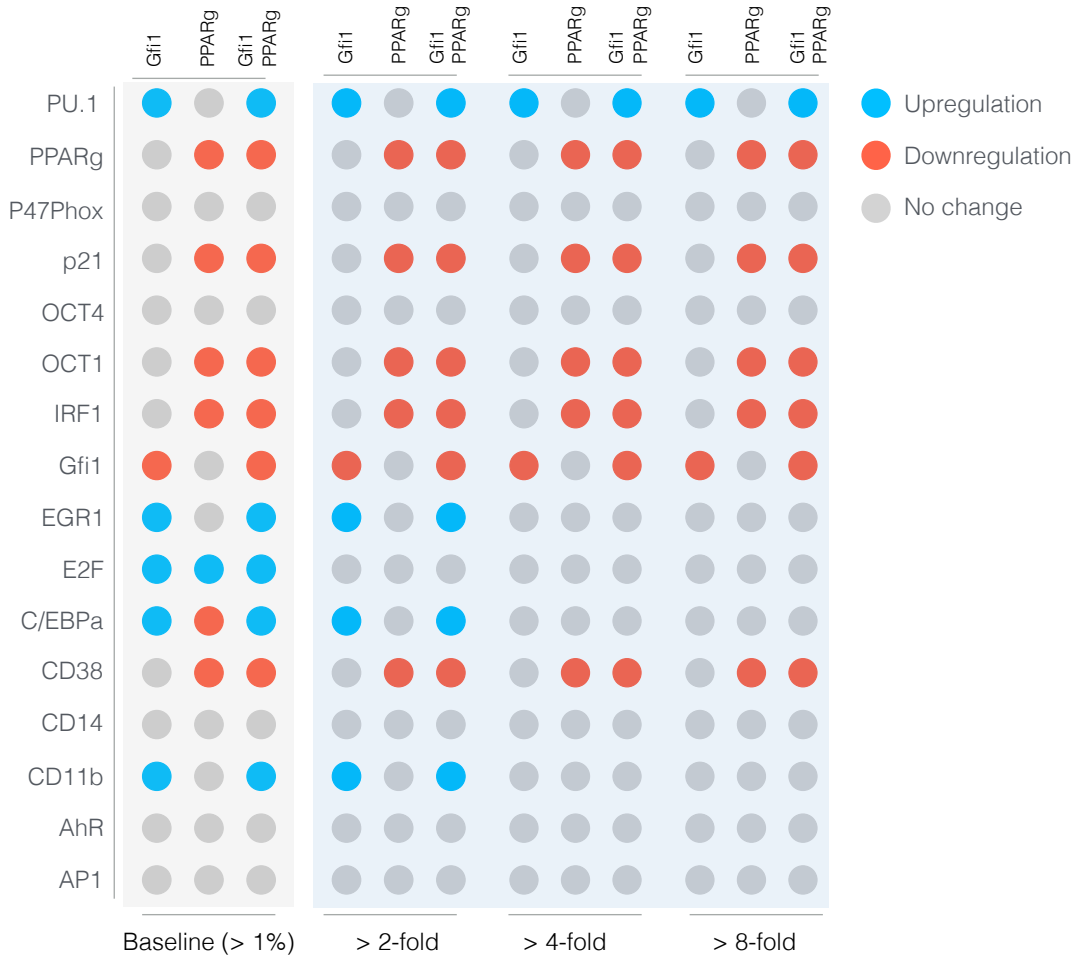


Fig. 7: Robustness of the HL-60 differentiation program following exposure to $1\mu\text{M}$ ATRA at $t = 0$ hr. Protein fold change at $t = 48$ hr (rows) in single and double knock-out mutants (columns) relative to wild-type HL-60 cells. The responses were grouped into $>2,4$ and 8 fold changes. The best fit parameter set was used to calculate the protein fold change.

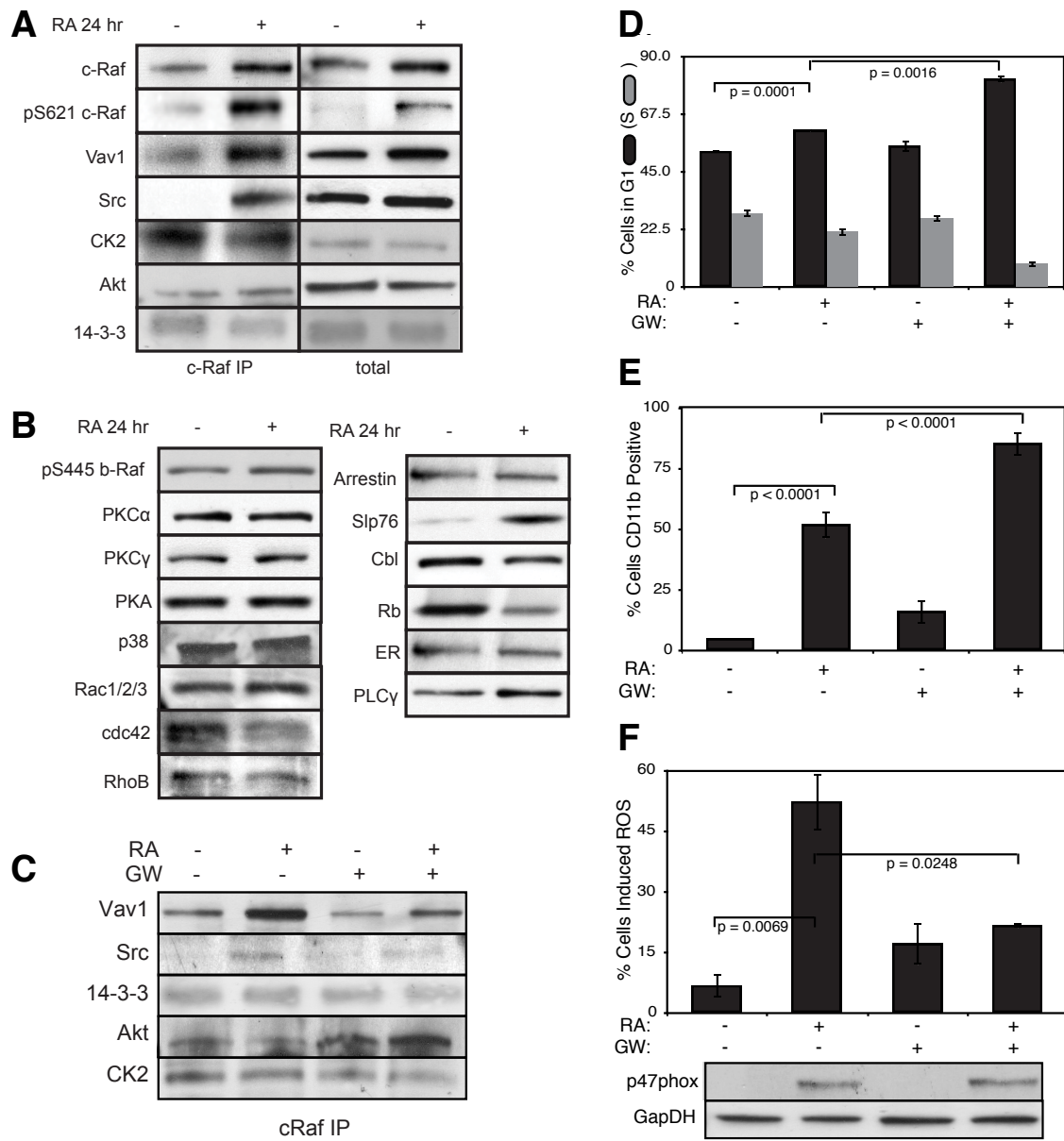


Fig. 8: Investigation of a panel of possible Raf interaction partners in the presence and absence of ATRA. A: Species identified to precipitate out with Raf: first column shows Western blot analysis on total Raf immunoprecipitation with and without 24 hr ATRA treatment and the second on total lysate. B: The expression of species considered that did not precipitate out with Raf at levels detectable by Western blot analysis on total lysate. C: Effect of the Raf inhibitor GW5074 on Raf interactions as determined by Western blot analysis of total Raf immunoprecipitation. The Authors note the signal associated with Src was found to be weak. D: Cell Cycle distribution as determined by flow cytometry indicated arrest induced by ATRA, which was increased by the addition of GW5074. E: Expression of the cell surface marker CD11b as determined by flow cytometry indicated increased expression induced by ATRA, which was enhanced by the addition of GW5074. F: Inducible reactive oxygen species (ROS) as determined by DCF flow cytometry. The functional differentiation response of ATRA treated cells was mitigated by GW5074.